NATIONAL ADVISORY COMMITTEE FOR AERONAUTICS

WARTIME REPORT

ORIGINALLY ISSUED

July 1942 as
Advance Confidential Report

PRELIMINARY INVESTIGATION IN THE NACA LOW-TURBULENCE TUNNEL OF LOW-DRAG AIRFOIL SECTIONS SUITABLE FOR ADMITTING AIR AT THE LEADING EDGE

By Albert E. von Doenhoff and Elmer A. Horton

Langley Memorial Aeronautical Laboratory
Langley Field, Va.

WASHINGTON

NATIONAL ADVISORY COMMITTEE FOR AERONAUTICS

ADVANCE CONFIDENTIAL REPORT

PRELIMINARY INVESTIGATION IN THE NACA LOW-TURBULENCE TUNNEL OF LOW-DRAG AIRFOIL SECTIONS SUITABLE FOR ADMITTING AIR AT THE LEADING EDGE

By Albert E. von Doenhoff and Elmer A. Horton

SUMMARY

An investigation was carried out in the NACA low-turbulence tunnel to develop low-drag airfoil sections suitable for admitting air at the leading edge. A thickness distribution having the desired type of pressure distribution was found from tests of a flexible model. Other airfoil shapes were derived from this original shape by varying the thickness, the camber, the leading-edge radius, and the size of the leading-edge opening.

Data are presented giving the characteristics of the airfoil shapes in the range of lift coefficients for high-speed and cruising flight. Shapes have been developed which show no substantial increase in drag over that of normal low-drag type sections having minimum pressure at the same position along the chord. Many of these shapes appear to have higher critical compressibility speeds than plain airfoils of the same thickness. Low-drag airfoil sections have been developed with openings in the leading edge as large as 41.5 percent of the maximum thickness. The range of lift coefficients for low drag in several cases is nearly as large as that of the corresponding plain airfoil sections.

Measurements of maximum lift characteristics were made for only a few configurations and no conclusions could be drawn as to what effect the leading-edge openings would have on the maximum lift characteristics of the complete wing.

INTRODUCTION

The leading edge of the wing has proved to be a convenient location for the entrance to air ducts. This location is potentially

efficient because the air can be brought to rest at this point without loss of total pressure. The placing of such openings in the leading edge of airfoils can lead, however, to serious increases in the external drag and to pressure peaks near the leading edge that can seriously reduce the critical compressibility speed. Even a very small peak, of course, eliminates the possibility of maintaining any extensive regions of laminar flow.

Previous tests in the NACA low-turbulence tunnel (unreported) showed the possibility of admitting air efficiently at the leading edge of low-drag-airfoil sections without disturbing the laminar layer. These tests, however, dealt with relatively small openings about 10 percent of the maximum thickness on an airfoil section of 21-percent thickness. In order to limit the span of the opening and to reduce duct losses, it is desirable to have as large an opening as possible and to admit the air at as low an intake-velocity ratio as possible. The purpose of the present investigation is the development of low-drag-airfoil sections having large openings in the leading edge.

In the development of the basic shapes, a model consisting of two flexible metal sheets fitted with pressure orifices was used. The model was mounted in the test section in such a manner that its shape could be altered from outside the tunnel while the effect on the pressure distribution could be observed on a multitube manometer. The entrance-flow rate was controlled by maintaining a fixed ratio of nose-to-tail openings. When the shape having the desired type of pressure distribution was obtained, the ordinates of the shape were measured and the pressure distribution was recorded. The ordinates of the symmetrical section obtained in this manner were plotted and faired; the faired ordinates were then used in the construction of a wooden model. A more detailed investigation of the characteristics of the airfoil section and the effect of various changes in shape was carried out with wooden models.

The present investigation deals primarily with the determination of section characteristics in the range of lift coefficients for high-speed and cruising flight. Although the importance of determining the effect of the use of these sections on the maximum lift of the wing is realized, it is felt that this effect can best be found from tests of a complete airplane model rather than from tests of a two-dimensional model of the nose-air intake section. Because the openings in the leading edge may extend over only a relatively small portion of the span, measurements of the maximum lift of the nose-opening sections alone would not give reliable information concerning the effect of the use of the sections on the complete airplane.

For this reason systematic measurements of section maximum lift coefficient have not been made; although some information on this subject has been obtained for a few conditions.

SYMBOLS

The symbols used are defined as follows:

V	free-stream velocity
V_n	velocity of air entering the nose opening
q	free-stream dynamic pressure $\left(\frac{1}{2}\rho V^2\right)$
p	local static pressure
H	free-stream total pressure
S	pressure coefficient $\left(\frac{H - p}{q}\right)$
H_t	total pressure at exit
ΔH	loss of total pressure through duct $(H - H_t)$
c_{d_o}	section profile-drag coefficient $\left(\frac{d_o}{qc}\right)$
c_l	section lift coefficient $\left(\frac{l}{qc}\right)$
α	angle of attack, degrees
δ_f	flap deflection, degrees
A_t	area of trailing-edge exit
A_n	area of leading-edge entrance
x	distance along chord from leading edge of airfoil
y	distance perpendicular to chord

c	chord
ρ	mass density
d_o	section drag
l	section lift
R	Reynolds number

APPARATUS AND METHODS

The investigation of low-drag airfoil sections reported herein was carried out in the NACA low-turbulence tunnel, which is designed to test models in two-dimensional flow. This tunnel has a test section 3 feet wide and $7\frac{1}{2}$ feet high. The turbulence level of the air stream in the tunnel is extremely low. Turbulence measurements with a hot-wire anemometer indicate that the fluctuations of velocity are less than 0.1 percent.

The flexible model, which consisted of two 0.024-inch-thick sheets of aluminum alloy, had a chord of 2 feet and a span of 3 feet. The sheets were mounted on eight 1/4-inch spanwise stringers that extended through the tunnel walls. Changes in the shape of the model could be made while the tunnel was running by changing the position of the stringers from outside the tunnel. On each surface of the model, at the midspan position, were 15 pressure orifices that were connected to a multitube manometer. A sketch of the model is given in figure 1. Although the flexible model was satisfactory for determining the outlines of the greater part of the section, it was not suitable for a study of the effects of changes near the leading edge. The internal shape furthermore did not make a suitable duct. Accordingly, the investigation was continued with the use of wooden models.

The wooden models were of 3-foot span and of approximately 24-inch chord or 60-inch chord. They were made in two sections, each section having a flexible metal trailing edge that could be used to adjust the size of the exit for varying the flow rate and as a split flap. The top and bottom sections were held together with 1/2-inch plywood end plates and several internal steel spacers. A photograph of a typical 60-inch-chord wooden model is shown in figure 2.

Pressure-distribution measurements were made on the flexible model by the use of the pressure orifices and on the wooden models by means of small static tubes of 0.040-inch outside diameter, mounted on supports approximately 0.25 inch above the model surface. Pressure distributions are presented as curves of the pressure coefficient S plotted against chordwise position. It is to be noted that, in forming this coefficient, free-stream total pressure is used as the reference pressure rather than free-stream static pressure. Surveys in a vertical plane at midspan indicated that the flow was more uniform at the exit than at the entrance. Measurements of flow were therefore made by measuring static pressure and total pressure at the center of the exit.

Drag was measured by the wake-survey method. The integral of the loss of total pressure in the wake, a fairly close approximation to the drag, was measured with an integrating manometer. Corrections to this value were obtained by a method substantially equivalent to that of B. M. Jones given in reference 1. The lift was determined from measurements of pressures along the floor and roof of the tunnel. Because the entire lift was not transferred to the tunnel walls within the distance covered by the orifices, a correction, determined theoretically, was applied to the measured results to obtain the total lift. The data presented herein have been corrected for tunnel-wall effects.

DEVELOPMENT OF NOSE-OPENING AIRFOIL SHAPES

Airfoil shape 7.- The measured ordinates of the flexible model were faired to obtain a symmetrical shape. The thickness of this symmetrical shape was then reduced to 16.900 percent c. Ordinates for this thickness distribution, called airfoil shape 7, are given in table I. The section was combined with an $a = 0.5$ type of mean line having a design lift coefficient of 0.2 to obtain the ordinates of the model. (See references 2 and 3.) The chord of the model was 24 inches.

The model was first tested with a sharp leading edge. The pressure distribution for this condition is given in figure 3. The slight peak in the pressure distribution on the lower surface near the leading edge, together with rather high values of the drag coefficient, indicated the

desirability of making some modifications to the leading edge. Rounding the leading edge to 1/32-inch radius resulted in the improved characteristics shown in figures 4 and 5.

In order to check the operation of the airfoil section in climb with an internal resistance to simulate a radiator, screens were installed that had a pressure drop equal to $\frac{5}{8}q$ when $\frac{V_n}{V}$ was equal to 0.9. Tests were made to determine whether this flow rate could be obtained at a lift coefficient of 0.8. For this series of measurements, the sheet-metal trailing edge on the lower surface was bent down, forming a 0.15c split flap. The characteristics were measured for flap deflections of $11\frac{1}{2}^\circ$, 15°, and 20°. The results are given in figure 6.

Tests to determine the maximum lift coefficient of the section when fitted with a 0.20c split flap deflected 60° were made in the NACA two-dimensional tunnel. The maximum lift coefficient showed little variation with Reynolds number. Removing the screens also had little effect. A typical lift curve showing the peak is given in figure 7.

Airfoil shape 8.- Airfoil shape 8 was derived from an improvement in the fairing of the ordinates of the flexible model used in deriving airfoil shape 7. No reduction was made in the thickness, however, which was the same as that of the flexible model, 18.892 percent c. The ordinates for the symmetrical model are given in table II. Figure 8 shows the shape of the airfoil section.

Tests of shape 8 with the sharp leading edge gave results similar to the initial results obtained for shape 7, indicating that the sharp leading edge was too critical. The leading edge was therefore rounded to approximately 1/32-inch radius (fig. 8). Figure 9 shows the pressure distribution for the model in this condition. Lift, drag, duct loss, and intake velocity were then measured. These results are given in figure 10 in nondimensional form.

In an effort to increase the low-drag range, the leading edge was cut back 2.489 percent c and was faired to a large radius (fig. 8). Ordinates are given in table III. Although this change improved the section characteristics (figs. 11 and 12), at least at low

Reynolds numbers, it affected the pressure distribution adversely near the leading edge, as is seen in figure 9. For succeeding models, a somewhat smaller leading-edge radius was therefore chosen.

Airfoil shape 9.- Airfoil shape 9 is the same as airfoil shape 8 except for the leading-edge radius, which is somewhat smaller than the large radius tested on shape 8. The ordinates for shape 9 are given in table IV. In order to obtain results at higher Reynolds numbers, the chord of this and of succeeding models was increased to 60 inches. Lift, drag, duct loss, intake velocity, and pressure distribution were measured for three different widths of the tail opening. These results are given in coefficient form in figures 13 to 15.

Airfoil shape 10.- Airfoil shape 10 resulted from an effort to fair an opening of a given size into an NACA 65,2-215 airfoil section with mean line $a = 0.8$ (reference 3) without changing the ordinates of the original section back of the 0.25c position. In order to avoid changing the shape of the mean line, a new symmetrical airfoil shape with the desired nose opening was derived, and this shape was cambered to the original mean line. This operation was performed by the use of shape 9, reduced somewhat in size, as a guide for the fairing in the neighborhood of the leading edge; this portion of the section was then faired into the NACA 65,2-015 section. A smooth curve was drawn by eye, joining the forward portion of the section with the NACA 65,2-015 section. In order to check the fairness of this curve, a measure of the curvature at several points along the surface was found, and this quantity was plotted against chordwise position. The measure of the curvature was computed according to the following formula

$$h_n = \frac{y_{(n-1)} + y_{(n+1)}}{2} - y_n$$

where y_n is the ordinate at the chordwise position x_n. The various chordwise positions x_1, x_2, ... x_n must be equally spaced. The original curve of h against x was not smooth. It was found necessary to make this curve smooth in order to obtain satisfactory pressure distributions. The curve of h against x was made smooth by successive arbitrary changes in the ordinates. The trailing edge was cut off at 0.91c to form the rear

opening. The resulting symmetrical section, designated airfoil shape 10, for which the ordinates are given in table V, was then cambered about an $a = 0.8$ type mean line with a design lift coefficient of 0.2 to obtain the ordinates of the model tested. The characteristics of this section were measured for three different widths of the trailing-edge opening. These results are given in figure 16.

In order to determine the effect of changing the angle between the line joining the upper- and lower-surface leading edges and the chord line, tests were made with the upper and lower surfaces shifted with respect to each other to give various amounts of stagger. The original stagger, due to the camber, was 0.265 inch. Tests were also made with staggers of 0.53 inch and 1.10 inches. Data for the tests with increased stagger are given in figures 17 and 18. The lift coefficient as a function of the angle of attack for the various test conditions is given in figure 19.

The results of pressure-distribution measurements for shape 10 are given in figure 20. Figure 21 gives a comparison between the theoretical pressure distribution for the NACA 65,2-015 airfoil section and the basic symmetrical pressure distribution derived from figure 20.

Airfoil shape 11.- Airfoil shape 11 is an airfoil section of approximately 0.25c maximum thickness. The ordinates were derived from those of airfoil shape 9 by increasing the ordinates for shape 9 in the ratio of the thicknesses of the shapes. The leading-edge radius was also increased by this ratio. Ordinates for airfoil shape 11 are given in table VI. The usual test results for this airfoil section are given in figures 22, 23, and 24.

Airfoil shape 12.- Airfoil shape 12 was derived to study the effect of variations in the size of the opening in the leading edge. Shape 12 has the same maximum thickness as shape 9, but the leading-edge opening has been reduced from approximately 32.5 percent of the maximum thickness to 23 percent of the maximum thickness. Ordinates for this shape are given in table VII. The test results are given in figures 25, 26, and 27.

Airfoil shape 13.- Airfoil shape 13 represents an effort to obtain an airfoil section having a very large opening in the leading edge. It was obtained by simply

spreading apart the upper and lower surfaces of airfoil shape 9. The resulting section had a maximum thickness of approximately 21.7 percent c and an opening in the leading edge of about 41.5 percent of the maximum thickness. Ordinates for shape 13 are given in table VIII. The test results are presented in figures 28 to 32.

DISCUSSION

Leading-edge radius.- As stated previously, satisfactory results were not obtained with the sharp leading edge. Comparison of figures 3 and 4 shows that the effect on the pressure distribution of slightly rounding the leading edge is to eliminate the peak on the lower surface.

Tests through a range of angle of attack, however, showed that the range of lift coefficients for low drag was very small. (See fig. 5.) In order to increase the range of lift coefficients for low drag, the leading edge was cut back considerably and rounded to a large radius as shown in figure 8. Although this change improved the low-drag range, as is seen in figure 11, it seems probable that this radius is too large because of its adverse effect on the pressure distribution shown in figure 9. It is believed that the low-drag range at higher Reynolds numbers would be considerably smaller than that shown in figure 11.

An intermediate value of the leading-edge radius was therefore chosen for airfoil shape 9. Although this value of the leading-edge radius may not be precisely the optimum, the data indicate that somewhat larger or smaller radii lead to characteristics less satisfactory than those for the intermediate radius.

Flow rate.- The effect of variations in the rate of air intake has been studied for a number of the airfoil sections. Air must be admitted at the leading edge in order to obtain satisfactory characteristics. The minimum rate of intake to obtain low drag, however, depends upon the particular section. For airfoil shape 9 with a leading-edge opening of about 32 percent of the maximum thickness, this minimum rate is a value of $\frac{V_n}{V}$ of approximately 0.38; for shape 12 with a leading-edge opening of

about 23 percent of the maximum thickness, it is less than 0.27. (See figs. 13(b), 13(c), and 25(c).)

In general, the characteristics of the sections improve with increase in the flow rate up to the point where the internal duct losses begin to be serious; that is, the low-drag range is increased and the value of the minimum pressure coefficient is reduced slightly as the flow rate is increased. It is noted that, although the low-drag range at first increases rapidly with increase in flow rate above the minimum necessary to obtain low drag as seen from the data for airfoil shapes 9 and 10 (figs. 13(b), 13(c), and 16), further increase in the flow rate has little effect as indicated by the data for shape 12 (fig. 25).

In all cases the loss of total pressure in the internal flow was negligible for a range of lift coefficients somewhat in excess of the low-drag range. Further increase in the lift coefficient resulted in a gradually increasing loss associated with local separation of the internal flow at the leading edge.

Airfoil thickness.- The effect of changing the thickness ratio can be seen from a comparison of the data for airfoil shapes 9 (figs. 13 to 15) and 11 (figs. 22 to 24). Increasing the thickness results in an increase of the low-drag range for a given ratio of opening to maximum thickness. Although the minimum pressure peak of shape 11 was higher than that of shape 9, the increase is not so much as would be expected from a corresponding increase in the thickness of a plain airfoil section. In this connection it should be noted that both shape 9 and shape 11 have considerably lower peak pressures than would be found on plain airfoil sections of the same thickness.

As previously stated, shape 11 was derived from shape 9 simply by multiplying the ordinates of shape 9 by the desired ratio of thicknesses. Another method of increasing the thickness is illustrated by shape 13. In this case the upper and lower surfaces were separated by a constant amount. The data for shape 13 (figs. 28 to 30) are very similar to those for shape 9, in spite of the fact that the thickness has been increased from about 19 to 22 percent and the ratio of the size of the leading-edge opening to the maximum thickness has been increased from approximately 32.5 to 41.5 percent. It is significant

that the peak pressure for shape 13 is practically the same as that for shape 9.

Size of leading-edge opening.- The effect of varying the size of the opening in the leading edge while the maximum thickness is kept constant can be seen from a comparison of the data for airfoil shapes 9 and 12 (figs. 13 to 15 and 25 to 27). Shape 9 has a leading-edge opening approximately 32.5 percent of the maximum thickness, and the opening in shape 12 is approximately 23 percent of the maximum thickness. The data indicate that the smaller opening is much less critical to flow rate and change of angle of attack than the larger opening. It is felt that shape 9 has about the largest-size opening in the leading edge that can be placed in a section of its thickness while still maintaining favorable aerodynamic characteristics.

There is some indication that the low-drag range is strongly influenced by the slope of the external contour in the neighborhood of the leading edge. Decreasing the size of the opening and increasing the thickness of the airfoil section both have the effect of increasing the slope near the leading edge. This larger slope has a tendency to increase the low-drag range. The conclusion should not be drawn, however, that this slope can be indefinitely increased, because it becomes difficult to fair the forward portion of the section into a shape of reasonable thickness without causing pressure peaks to occur a short distance from the leading edge.

Pressure distribution.- Comparison of the pressure distributions for the various shapes with those for plain airfoils of corresponding thicknesses shows that the values of the minimum pressure coefficient for many of the nose-opening shapes are considerably lower than those for the plain airfoils. As an example, airfoil shape 13, which is 21.774 percent thick, has approximately the same value of the minimum pressure coefficient as the NACA 66,2-016 airfoil section at zero lift. A lower value of the peak pressure is of importance because it indicates an increase in the critical compressibility speed of the section. This increase enables the designer to use a thicker section than would otherwise prove feasible.

The theoretical pressure distributions given for comparison with those for the various nose-opening shapes are the pressure distributions for NACA low-drag airfoils having the same thickness ratio as those of the nose-opening shapes, except in the case of shape 10. Figure

21 gives a comparison between airfoil shape 10 and the NACA 65,2-015 airfoil section. In this figure the trailing edge of shape 10 corresponds to a value of 0.91 for x/c, and the trailing edge of the NACA 65,2-015 airfoil corresponds to a value of 1.0 for x/c. The actual thickness ratio of shape 10 is, of course, greater than 0.15 because the chord has been decreased by 9 percent. This comparison shows that the minimum pressure coefficient for a nose-opening shape is very nearly the same as that of the plain section into which it fairs; that is, no considerable increases in critical compressibility speeds are to be expected from nose-opening sections derived by modifying only the leading edge of the original plain airfoil section.

Maximum lift.- As stated in the Introduction, it is felt that the effect of nose-opening sections on maximum lift can best be found from tests of a complete airplane model rather than from tests of a two-dimensional model of the nose-air intake section. Such tests have not yet been made. Some preliminary checks, however, indicate that the possible decreases in maximum lift should not be large. The maximum lift of airfoil shape 7 when fitted with a 20-percent-chord split flap deflected 60° is seen from figure 7 to be 2.15. Measurements of the maximum lift of shape 11 cambered for a design c_l of 0.4 with an a = 1.0 type mean line gave a value of 1.41 at a Reynolds number of 6×10^6 as compared with 1.42 at the same Reynolds number for an NACA 65,2-422 airfoil section with an a = 1.0 type mean line. The maximum lift of an NACA 65,2-215, a = 0.8, airfoil section was measured with nose-opening shape 10 extending over approximately 11 percent of the span of the model. No change in the maximum lift was observed in this case. Such data, however, are too incomplete to draw any conclusions as to the possible effect of leading-edge openings on the maximum lift characteristics of the complete wing.

Drag.- The values of the drag coefficient of nose-opening sections in the low-drag range are practically the same as those of the corresponding low-drag sections. Figure 31 gives a comparison between airfoil shape 10 and the NACA 65,2-215 airfoil section. It is seen that the low-drag range is somewhat less than that of the original section and that the drag outside of the low-drag range increases at a greater rate with lift coefficient than for the plain section. A large part of this increase in drag is due to the internal losses that occur at angles of attack outside of the low-drag range. The data indicate that the low-drag range increases (a) with increasing flow rate, (b) with decreasing entrance size for sections of a given thickness, and (c) with increasing thickness if the ratio of the width of the opening to the maximum thickness

is maintained constant. Of the shapes tested, the largest low-drag range was shown by shape 11 with a lift-coefficient range for low drag of 0.4 with a $\frac{V_n}{V}$ of 0.48 (fig. 22(a)).

Application.- It appears from the present data that the proper use of the nose-opening sections presented in this report can lead to cooling installations having practically no additional external drag in the range of lift coefficients for high-speed and cruising flight. Although most of the airfoil shapes for which data are given are symmetrical, these shapes can be treated in the same manner as any other low-drag type symmetrical sections; that is, the symmetrical shapes can be combined with a mean line having the desired design lift in order to shift the range of lift coefficients for low drag and efficient internal flow, as is indicated by the data for shape 10. (See fig. 16(a).) Staggering the opening had an effect similar to the effect of an increase in the camber, only smaller. Results showing the effect of various amounts of stagger are given in figures 16(b), 17, and 18.

If it is desired to fair nose-opening shapes into existing airfoil sections, it is recommended that a procedure similar to that used in the derivation of shape 10 be employed. In particular, it is usually desirable not to alter the shape of the original mean line and to be certain that the variation of curvature along the surface is smooth and continuous.

Because the amount of air required for cooling in the climb condition is nearly as much as is required in the high-speed condition, the intake-velocity ratio in the climb condition must be considerably greater than for the high-speed conditions. Tests of airfoil shape 7 with an internal resistance having a pressure drop of $\frac{5}{8}q$ at an intake-velocity ratio $\frac{V_n}{V}$ of 0.9 showed the possibility of obtaining high intake-velocity ratios at high lift coefficients. Interpolation of the results given in figure 6 shows that a flow rate $\frac{V_n}{V}$ of 0.9 can be obtained at a lift coefficient of 0.8 with a combined cooling control and a split flap deflected 17.2°. An analysis of the drag data obtained from this series of tests indicates that the external drag caused by deflection of the flap is much less than that ordinarily associated with the deflection of a split flap; in fact, the increase in total drag is the increase that could be associated with the internal losses. This result is reasonable because the flow over the upper surface of the flap was not stalled.

A few short tests were made to determine suitable methods of ending the opening and fairing the nose-opening shape into the wing in the spanwise direction. These tests indicated that the opening should be closed gradually in a length equal to at least twice the maximum height of the opening. Semicircular or elliptical ends were unsatisfactory.

CONCLUSIONS

1. Airfoil sections of the low-drag type, suitable for admitting air at the leading edge without substantial increase in drag, have been developed.

2. Many of the sections tested appear to have higher critical compressibility speeds than plain sections of the same thickness.

3. Low-drag sections have been developed that have openings in the leading edge as large as 41.5 percent of the maximum thickness.

4. The range of lift coefficients for low drag in several cases is nearly as large as that of the corresponding plain airfoil section.

5. The measurements of maximum lift characteristics were too incomplete to draw any conclusions regarding the effect of leading-edge openings on the maximum lift characteristics of the complete wing.

Langley Memorial Aeronautical Laboratory,
National Advisory Committee for Aeronautics,
Langley Field, Va.

REFERENCES

1. The Cambridge University Aeronautics Laboratory: The Measurement of Profile Drag by the Pitot-Traverse Method. R. & M. No. 1688, British A.R.C., 1936.

2. Jacobs, Eastman N., Abbott, Ira H., and Davidson, Milton: Preliminary Low-Drag-Airfoil and Flap Data from Tests at Large Reynolds Numbers and Low Turbulence. NACA A.C.R., March 1942.

3. Jacobs, Eastman N., Abbott, Ira H., and Davidson, Milton: Supplement to Advance Confidential Report, Preliminary Low-Drag-Airfoil and Flap Data from Tests at Large Reynolds Numbers and Low Turbulence. Black loose-leaf notebook dated March 1942.

TABLE I

THICKNESS ORDINATES, NOSE-OPENING

AIRFOIL SHAPE 7

x (percent c)	y (percent c)
0	2.753
.5	3.154
.75	3.292
1.25	3.559
2.5	4.110
5.0	4.925
7.5	5.440
10	5.880
15	6.608
20	7.188
25	7.612
30	7.935
35	8.222
40	8.388
45	8.450
50	8.410
55	8.210
60	7.808
65	7.228
70	6.520
75	5.677
80	4.770
85	3.872
90	2.960
95	2.040
100	1.250
Nose opening in percent of maximum thickness: 32.580	

TABLE II

THICKNESS ORDINATES, SHARP-LEADING-EDGE

NOSE-OPENING AIRFOIL SHAPE 8

x (percent c)	y (percent c)
0	3.000
.5	3.451
.75	3.625
1.25	3.935
2.5	4.500
5.0	5.352
7.5	5.978
10	6.505
15	7.353
20	8.000
25	8.478
30	8.902
35	9.222
40	9.386
45	9.446
50	9.348
55	9.159
60	8.913
65	8.484
70	7.793
75	6.843
80	5.807
85	4.745
90	3.701
95	2.402
100	1.339
Nose opening in percent of maximum thickness: 31.760	

TABLE III

THICKNESS ORDINATES, LARGE LEADING-EDGE-RADIUS

NOSE-OPENING AIRFOIL SHAPE 8

x (percent c)	y (percent c)
2.489	3.413
2.60	3.772
2.8	4.038
3.0	4.245
4.0	4.908
5.0	5.337
7.5	5.978
10	6.505
15	7.353
20	8.000
25	8.478
30	8.902
35	9.222
40	9.386
45	9.446
50	9.348
55	9.159
60	8.913
65	8.484
70	7.793
75	6.843
80	5.807
85	4.745
90	3.701
95	2.402
100	1.339
Location of leading-edge radius: 2.772	3.413
Leading-edge radius: 0.283 percent c	
Nose opening in percent of maximum thickness: 33.136	

TABLE IV

THICKNESS ORDINATES, NOSE-OPENING

AIRFOIL SHAPE 9

x (percent c)	y (percent c)
0	3.343
.5	3.835
.75	3.976
1.25	4.228
2.5	4.745
5.0	5.532
7.5	6.137
10	6.652
15	7.467
20	8.098
25	8.593
30	8.965
35	9.224
40	9.379
45	9.435
50	9.391
55	9.240
60	8.966
65	8.510
70	7.804
75	6.878
80	5.816
85	4.679
90	3.522
95	2.387
100	1.314
Leading-edge radius: 0.251 percent c	
Location of leading-edge radius center: 0.251	3.343
Location of fairing point in opening: 0.407	3.067
Nose opening in percent of maximum thickness: 32.507	

TABLE V

THICKNESS ORDINATES, NOSE-OPENING

AIRFOIL SHAPE 10

x (percent c)	y (percent c)
0	2.001
.5	2.409
.75	2.546
1.25	2.785
2.5	3.264
5.0	3.979
7.5	4.552
10	5.064
15	5.944
20	6.660
25	7.235
30	7.678
35	7.993
40	8.180
45	8.240
50	8.163
55	7.906
60	7.439
65	6.798
70	6.030
75	5.182
80	4.286
85	3.369
90	2.452
95	1.616
100	.877
Leading-edge radius: 0.151 percent c	
Location of leading-edge radius center: 0.151	2.001
Location of fairing point in opening: 0.244	1.836
Nose opening in percent of maximum thickness: 22.282	

TABLE VI

THICKNESS ORDINATES, NOSE-OPENING

AIRFOIL SHAPE 11

x (percent c)	y (percent c)
0	4.404
.5	5.052
.75	5.238
1.25	5.570
2.5	6.251
5.0	7.287
7.5	8.084
10	8.763
15	9.836
20	10.668
25	11.320
30	11.810
35	12.151
40	12.355
45	12.429
50	12.371
55	12.172
60	11.811
65	11.210
70	10.280
75	9.060
80	7.661
85	6.164
90	4.640
95	3.144
100	1.731
Leading-edge radius: 0.331 percent c	
Location of leading-edge radius center: 0.331	4.404
Location of fairing point in opening: 0.536	4.040
Nose opening in percent of maximum thickness: 32.505	

TABLE VII

THICKNESS ORDINATES, NOSE-OPENING

AIRFOIL SHAPE 12

x (percent c)	y (percent c)
0	2.378
.5	3.163
.75	3.352
1.25	3.667
2.5	4.264
5.0	5.141
7.5	5.819
10	6.392
15	7.291
20	7.982
25	8.521
30	8.925
35	9.206
40	9.375
45	9.435
50	9.391
55	9.240
60	8.966
65	8.510
70	7.804
75	6.878
80	5.816
85	4.679
90	3.522
95	2.387
100	1.314
Leading-edge radius: 0.179 percent c	
Location of leading-edge radius center 0.179	2.378
Location of fairing point in opening: 0.290	2.182
Nose opening in percent of maximum thickness: 23.122	

TABLE VIII

THICKNESS ORDINATES, NOSE-OPENING

AIRFOIL SHAPE 13

x (percent c)	y (percent c)
0	4.795
.5	5.287
.75	5.428
1.25	5.680
2.5	6.197
5.0	6.984
7.5	7.589
10	8.104
15	8.919
20	9.550
25	10.045
30	10.417
35	10.676
40	10.821
45	10.887
50	10.843
55	10.692
60	10.418
65	9.962
70	9.256
75	8.330
80	7.268
85	6.131
90	4.974
95	3.839
100	2.766
Leading-edge radius: 0.251 percent c	
Location of leading-edge radius center: 0.251	4.795
Location of fairing point in opening: 0.407	4.519
Nose opening in percent of maximum thickness: 41.508	

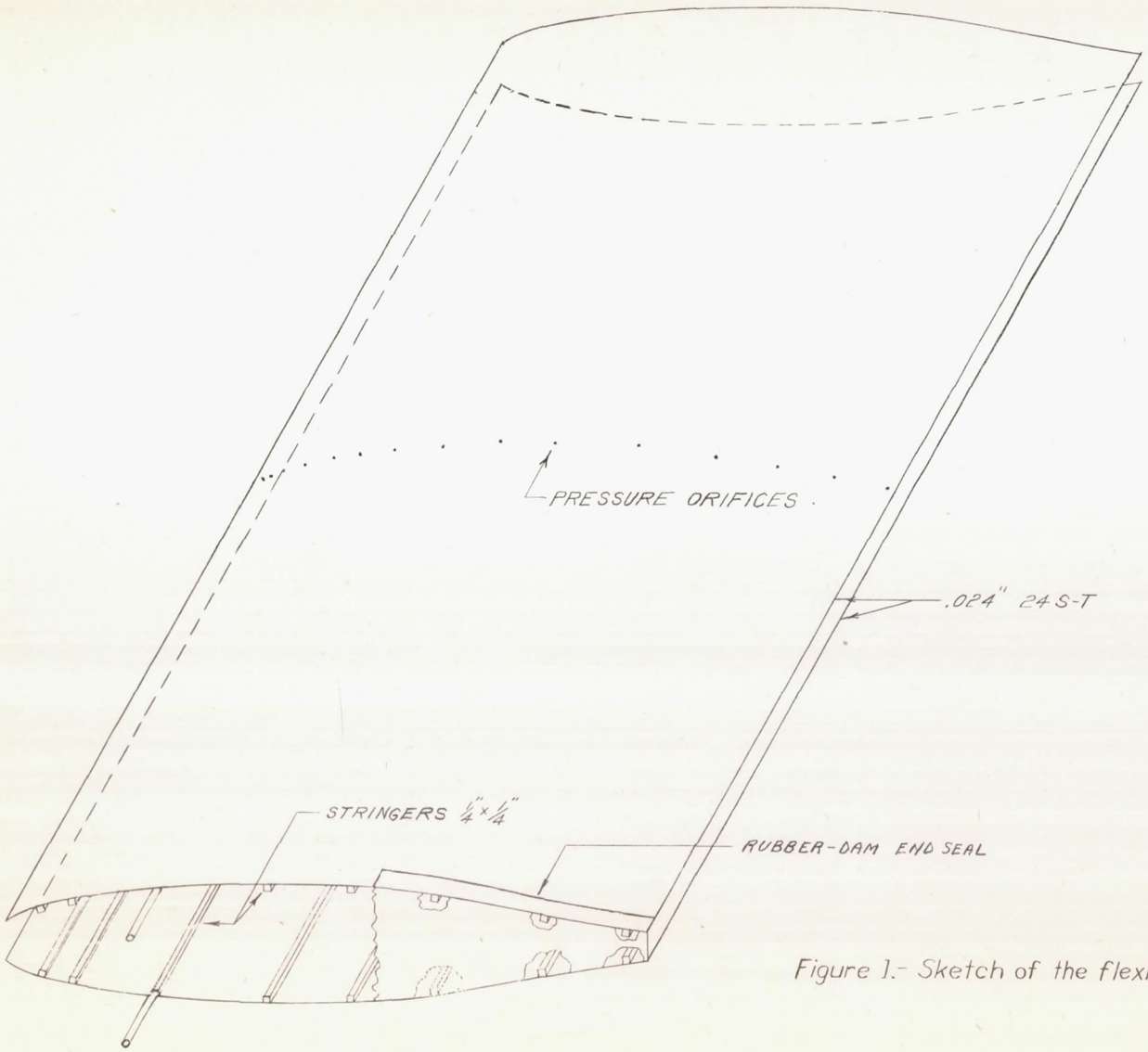

Figure 1.- Sketch of the flexible airfoil shape.

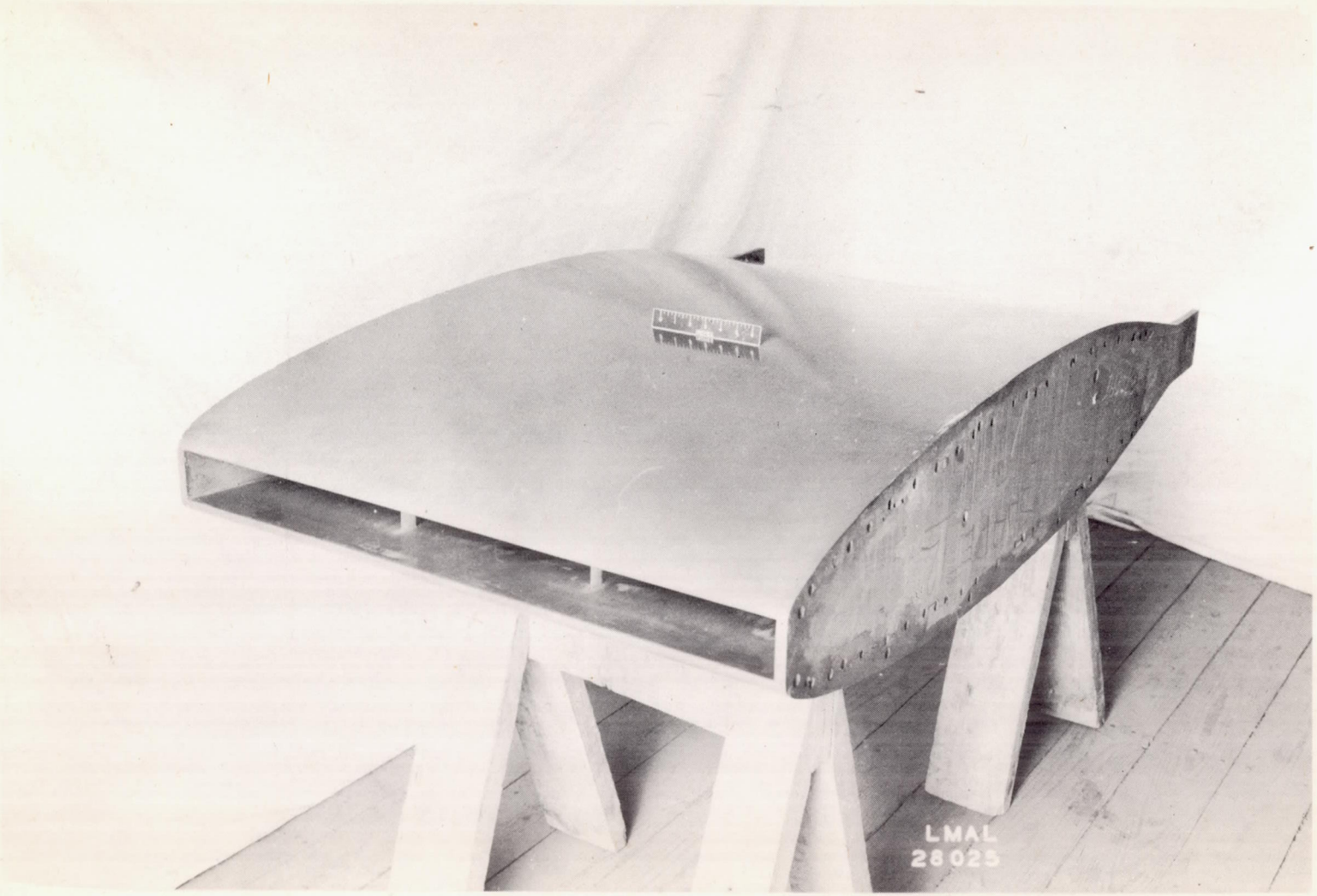

Figure 2.- View showing typical 60-inch-chord nose-opening model.

L-694

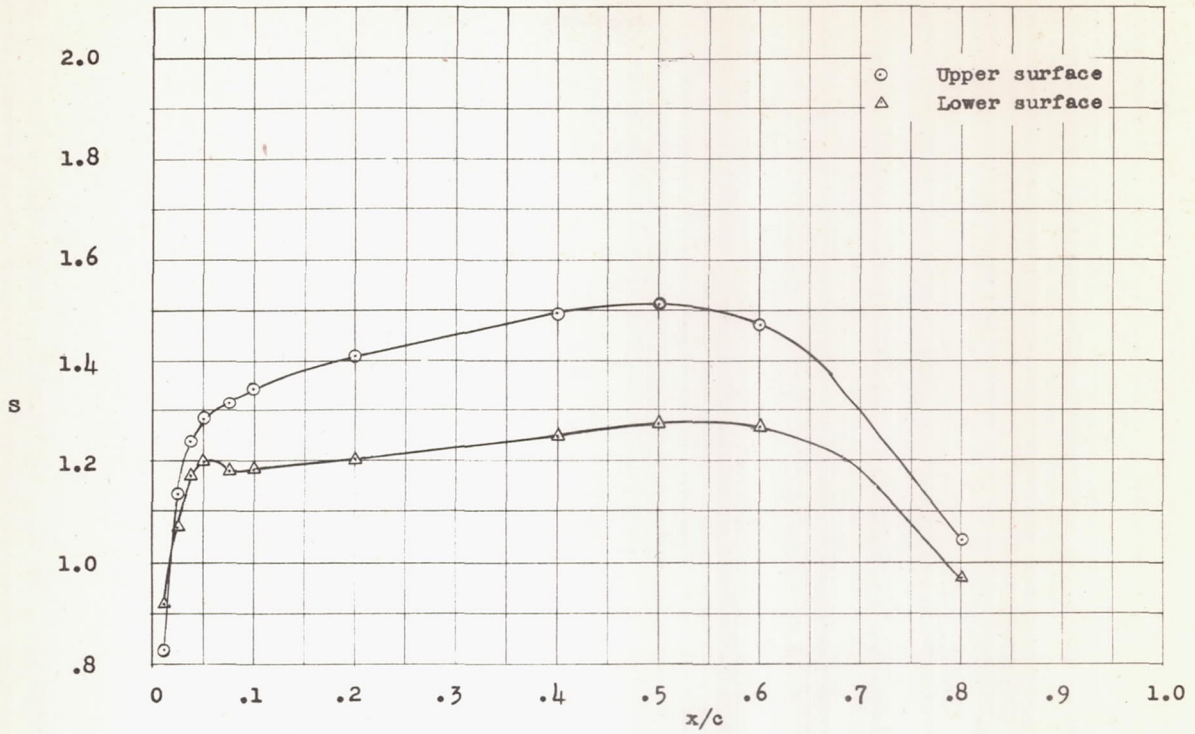

Figure 3.- Pressure distribution for airfoil shape 7 cambered for c_l = 0.2 with sharp leading edge. α, 0°; V_n/V, 0.426; A_t/A_n, 0.439; R, 2.02 × 10^6.

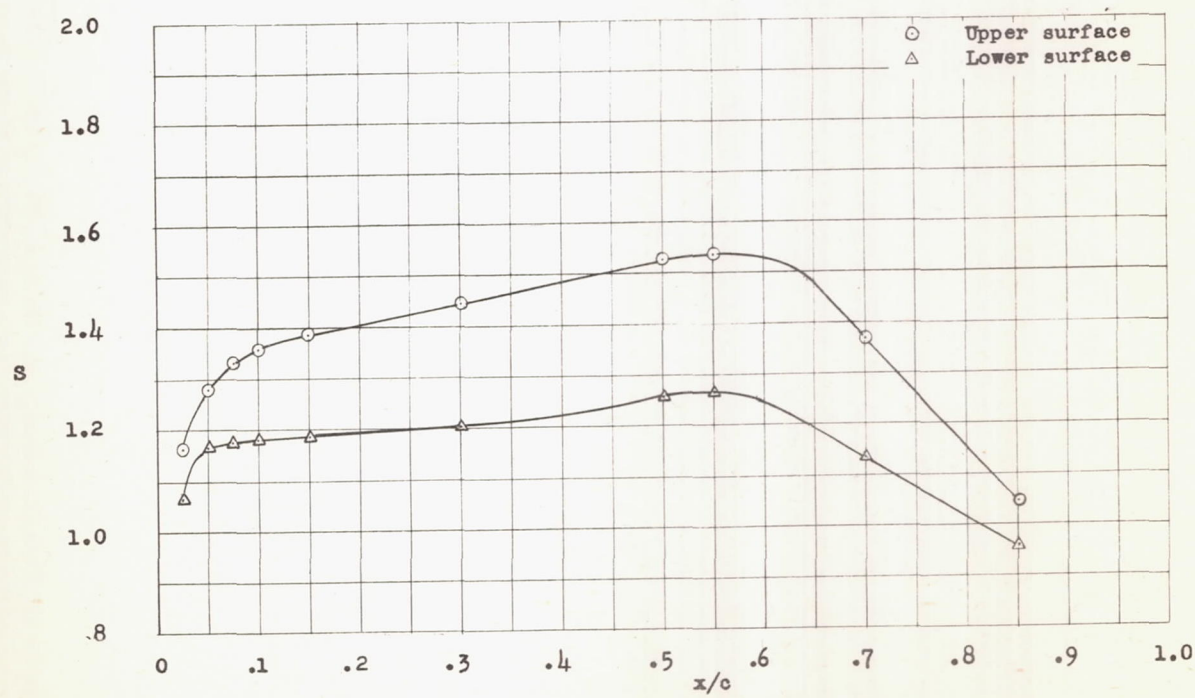

Figure 4.- Pressure distribution for airfoil shape 7 cambered for c_l = 0.2. Leading-edge radius, 1/32-inch; α, 0°; V_n/V, 0.426; A_t/A_n, 0.439; R, 2.02 × 10^6.

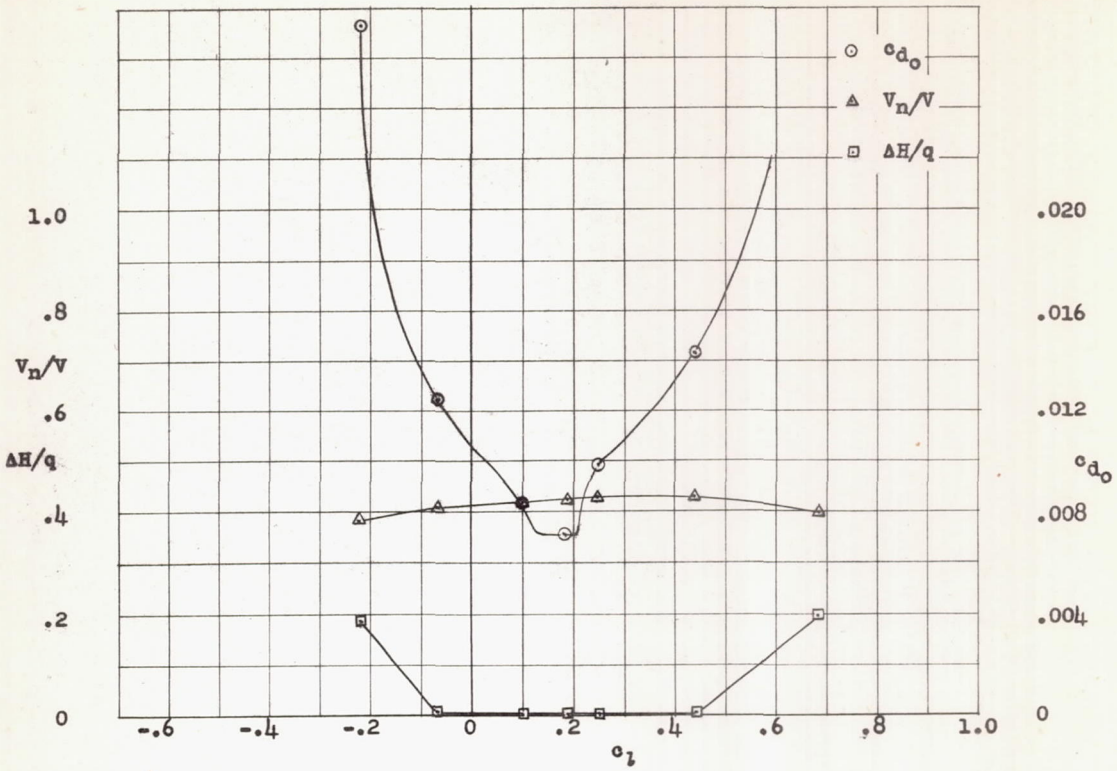

Figure 5.- Section characteristics for airfoil shape 7 cambered for $c_l = 0.2$. Small leading-edge radius. α, 0°; A_t/A_n, 0.439; R, 2.25×10^6.

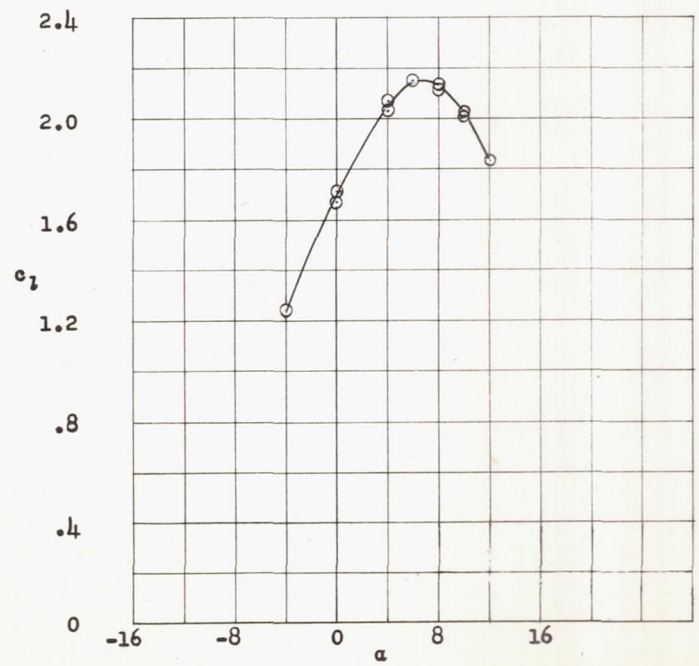

Figure 7.- Section lift coefficients for airfoil shape 7 cambered for $c_l = 0.2$ with 0.20c split flap deflected 60°. Two 30-mesh screens to simulate cooling resistance. R, 3.13×10^6.

L-694

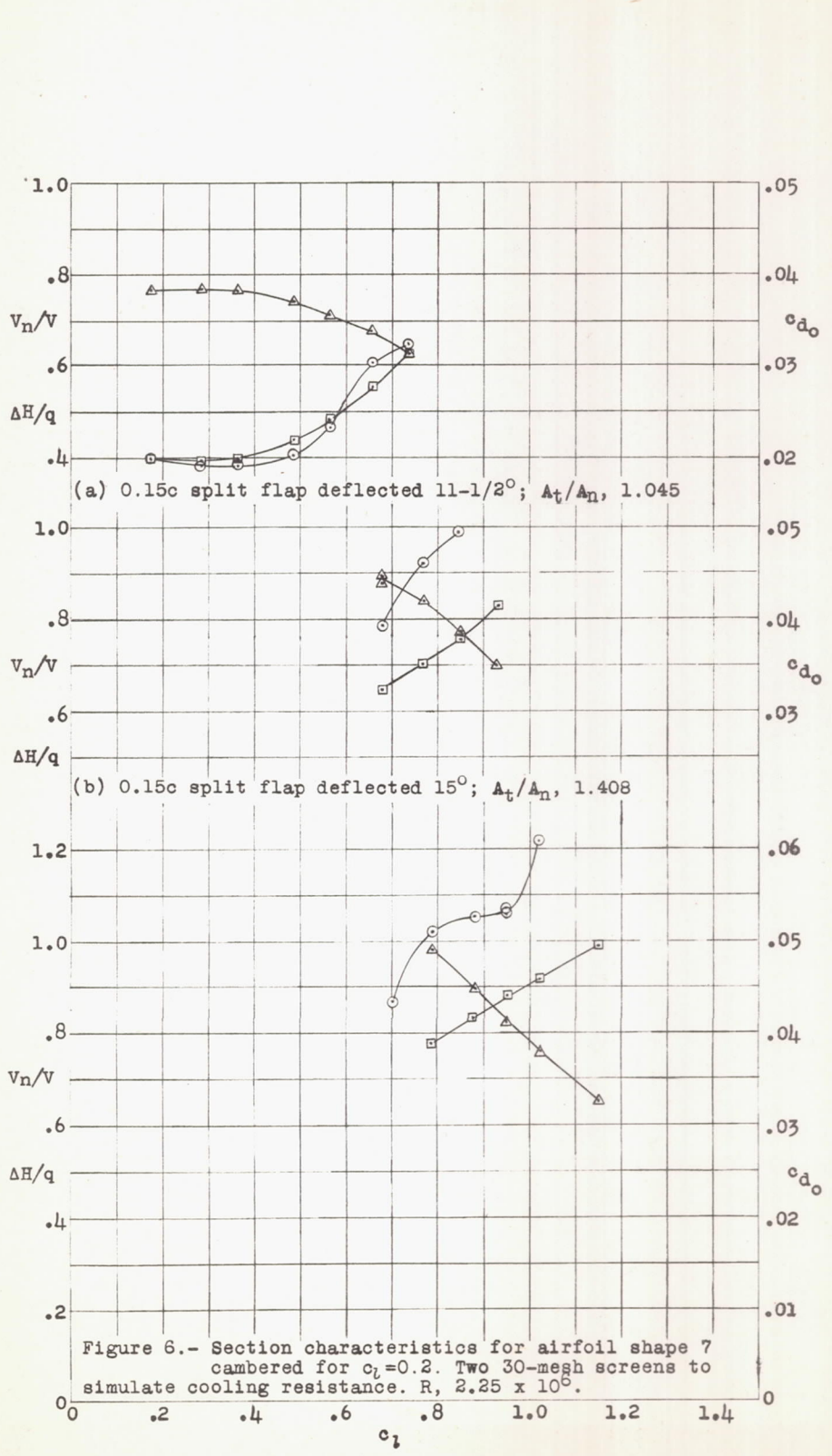

(a) 0.15c split flap deflected 11-1/2°; A_t/A_n, 1.045

(b) 0.15c split flap deflected 15°; A_t/A_n, 1.408

Figure 6.- Section characteristics for airfoil shape 7 cambered for c_l=0.2. Two 30-mesh screens to simulate cooling resistance. R, 2.25 x 10^6.

(c) 0.15c split flap deflected 20°; A_t/A_n, 1.697.

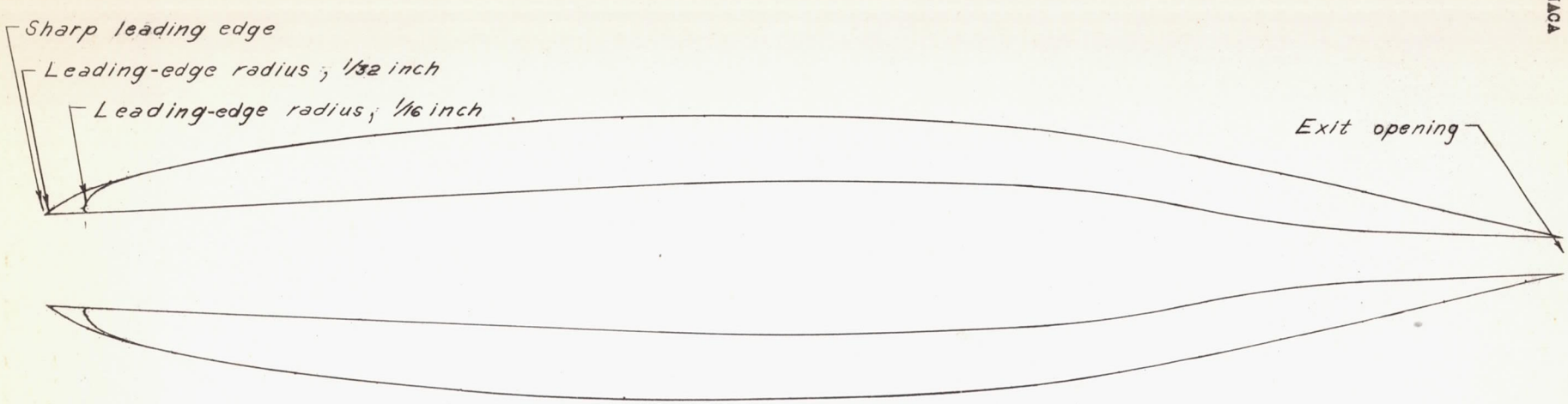

Figure 8.- Airfoil shape 8 showing several leading-edge shapes and typical internal duct.

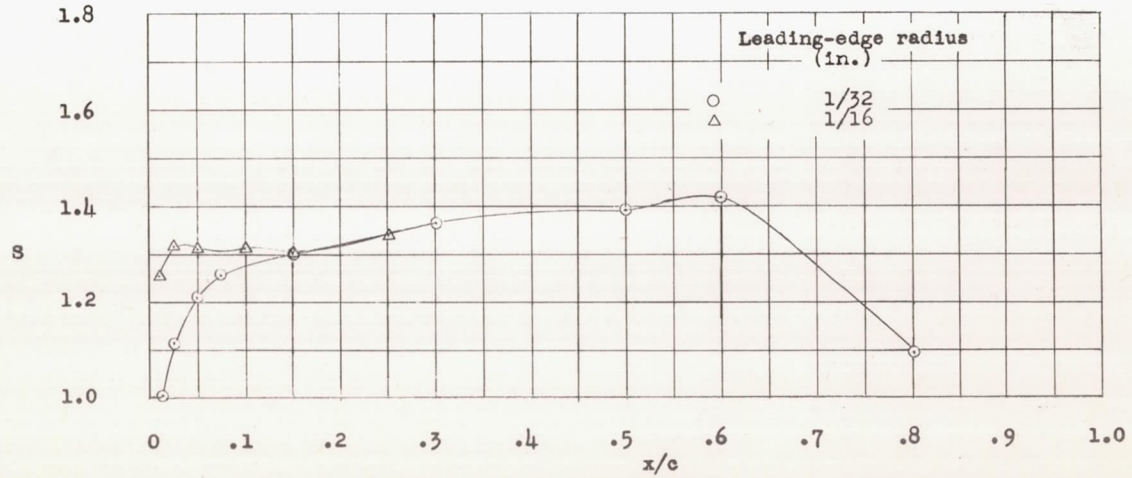

Figure 9.- Pressure distributions for airfoil shape 8. α, 0°; V_n/V, 0.465; A_t/A_n, 0.536; R, 2.00×10^6.

L-694

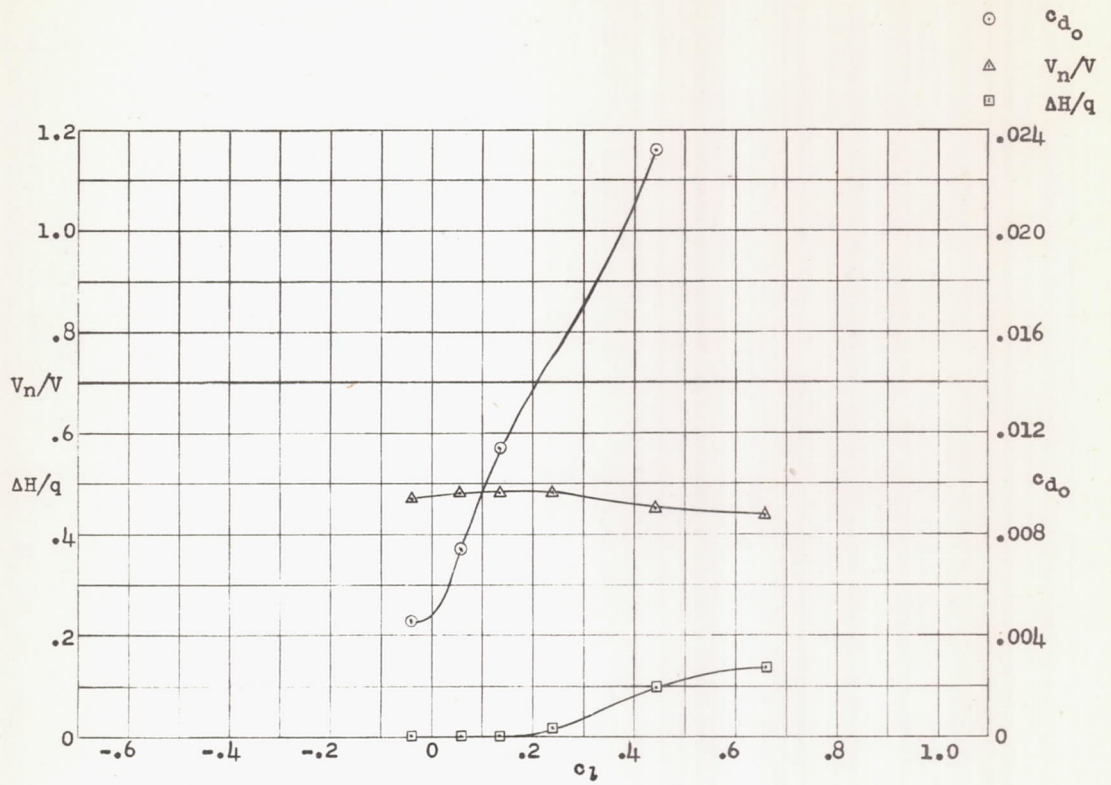

Figure 10.- Section characteristics for airfoil shape 8 with small nose radius. A_t/A_n, 0.536; R, 2.27 × 10^6.

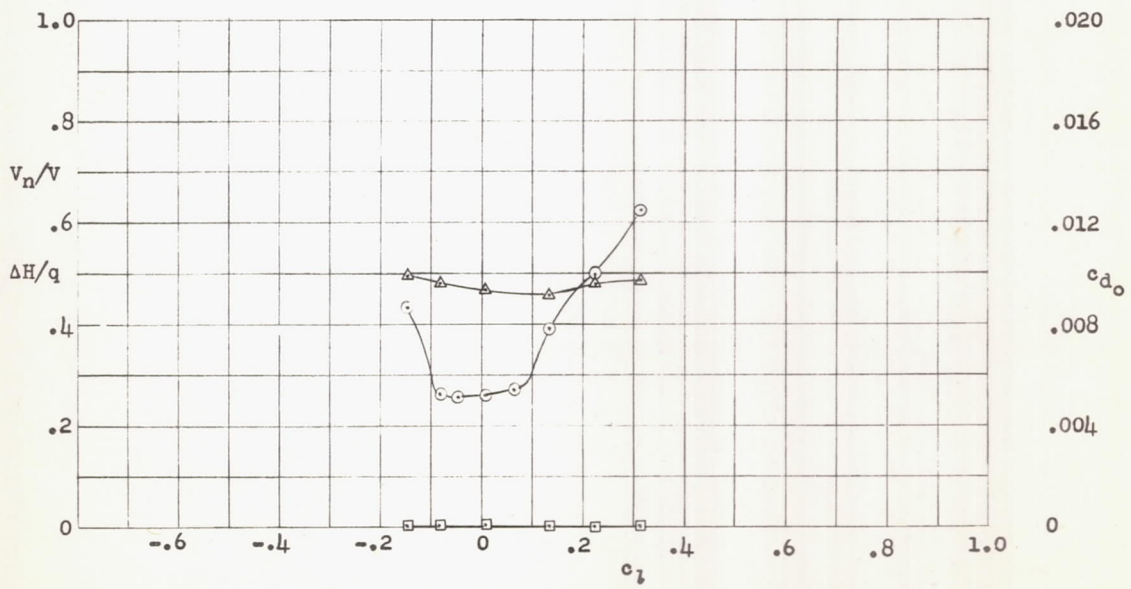

Figure 11.- Section characteristics for airfoil shape 8 with large nose radius. A_t/A_n, 0.536; R, 2.27 × 10^6.

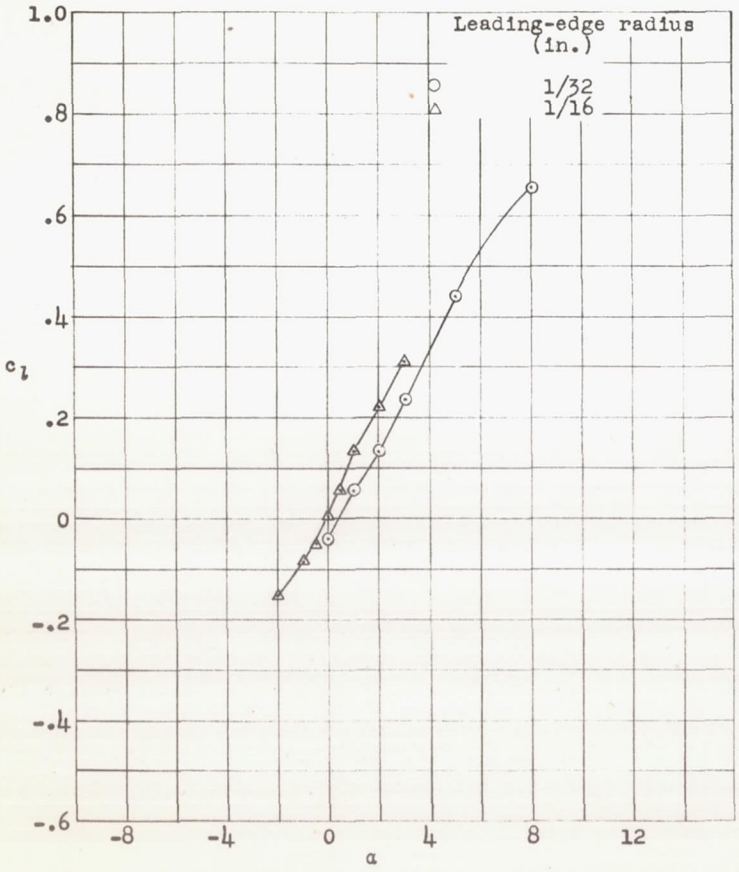

Figure 12.- Section lift coefficients for airfoil shape 8 with small and large nose radii. A_t/A_n, 0.536; R, 2.27×10^6.

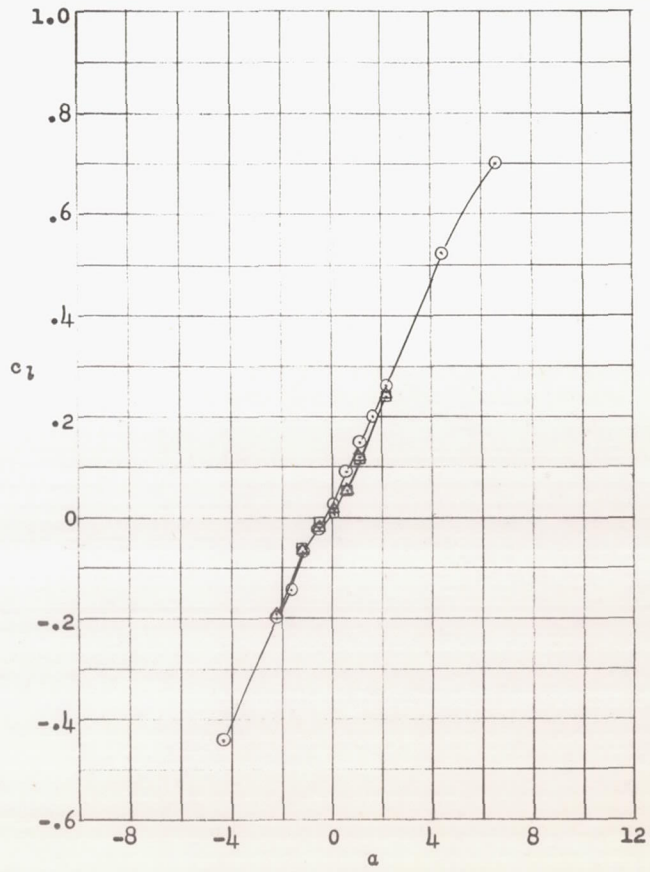

Figure 14.- Section lift coefficients for airfoil shape 9 for various flow rates. R, 6.43×10^6.

L-694

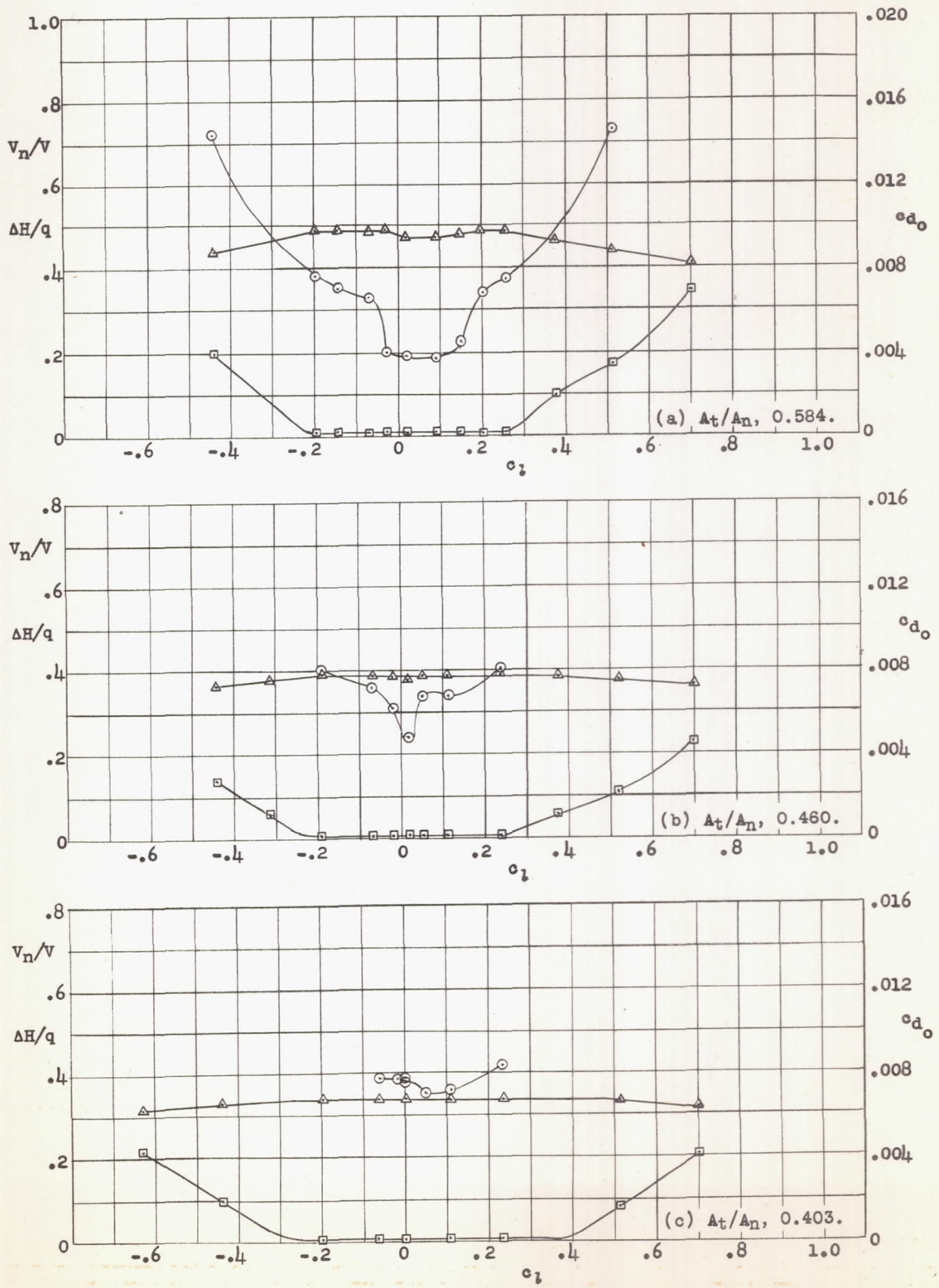

Figure 13.- Section characteristics for airfoil shape 9. R, 6.43×10^6.

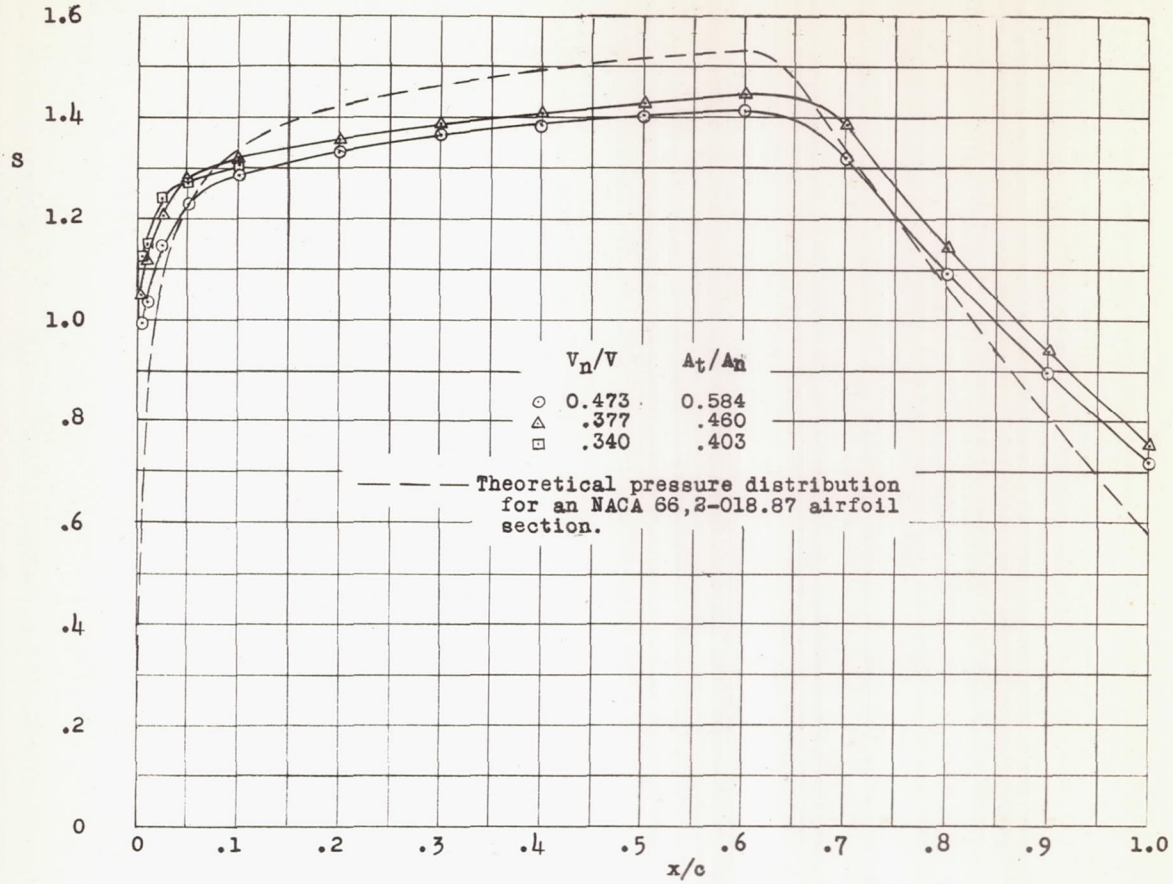

Figure 15.- Pressure distributions for airfoil shape 9. α, 0°; R, 6.43 × 10^6.

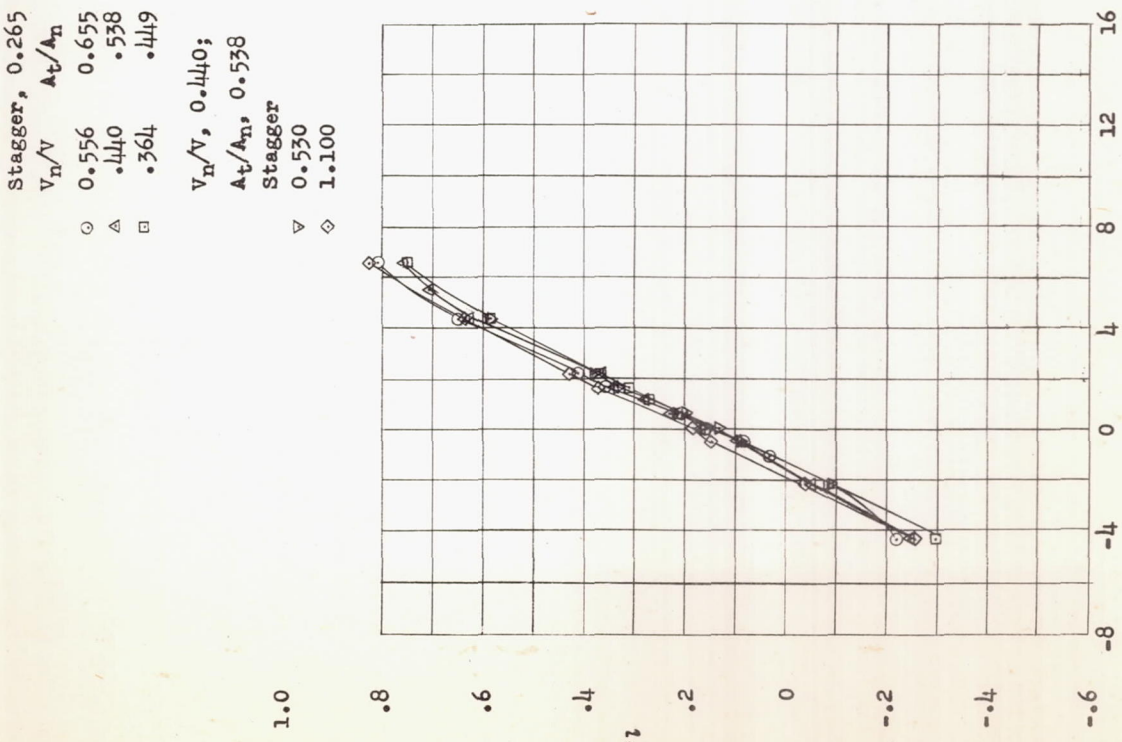

Figure 19.- Section lift coefficients for airfoil shape 10 for various test conditions. R, 6.43 × 10^6.

Figs. 16a,b

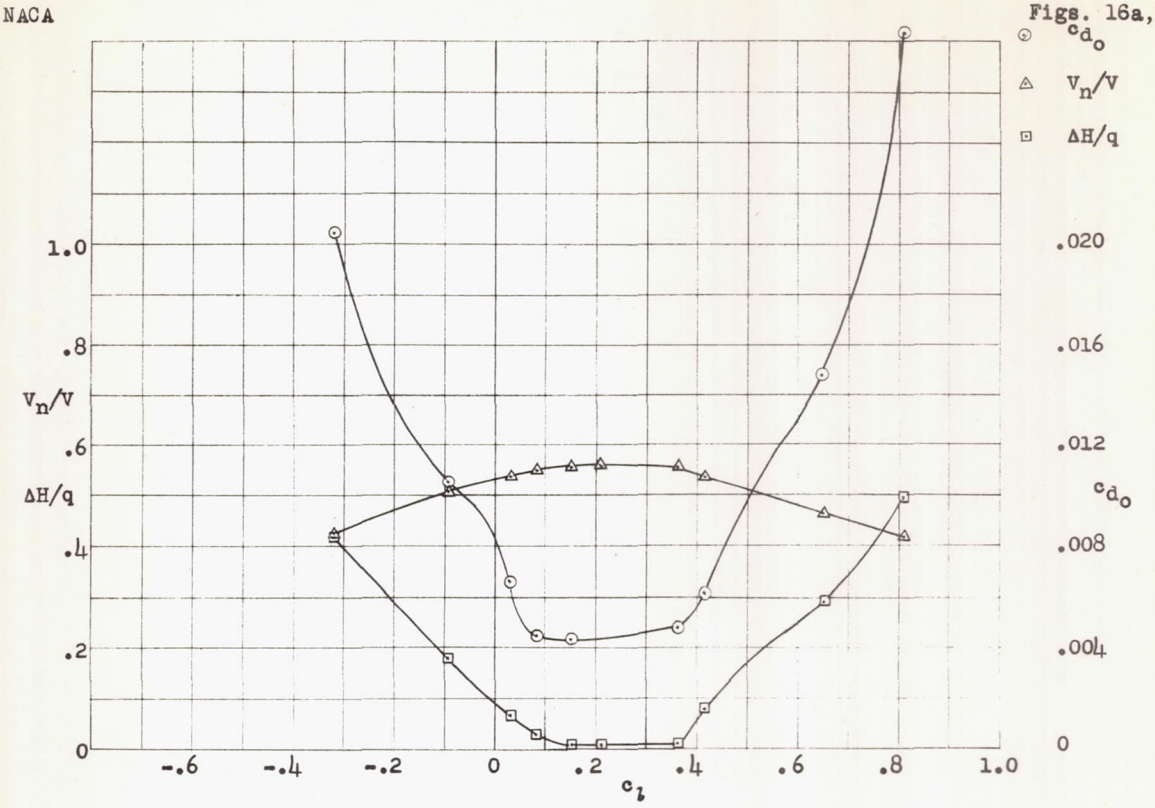

(a) A_t/A_n, 0.655.

Figure 16.- Section characteristics for airfoil shape 10 at R = 6.43 × 10^6 and with a stagger of 0.265 inch. (a,b,c)

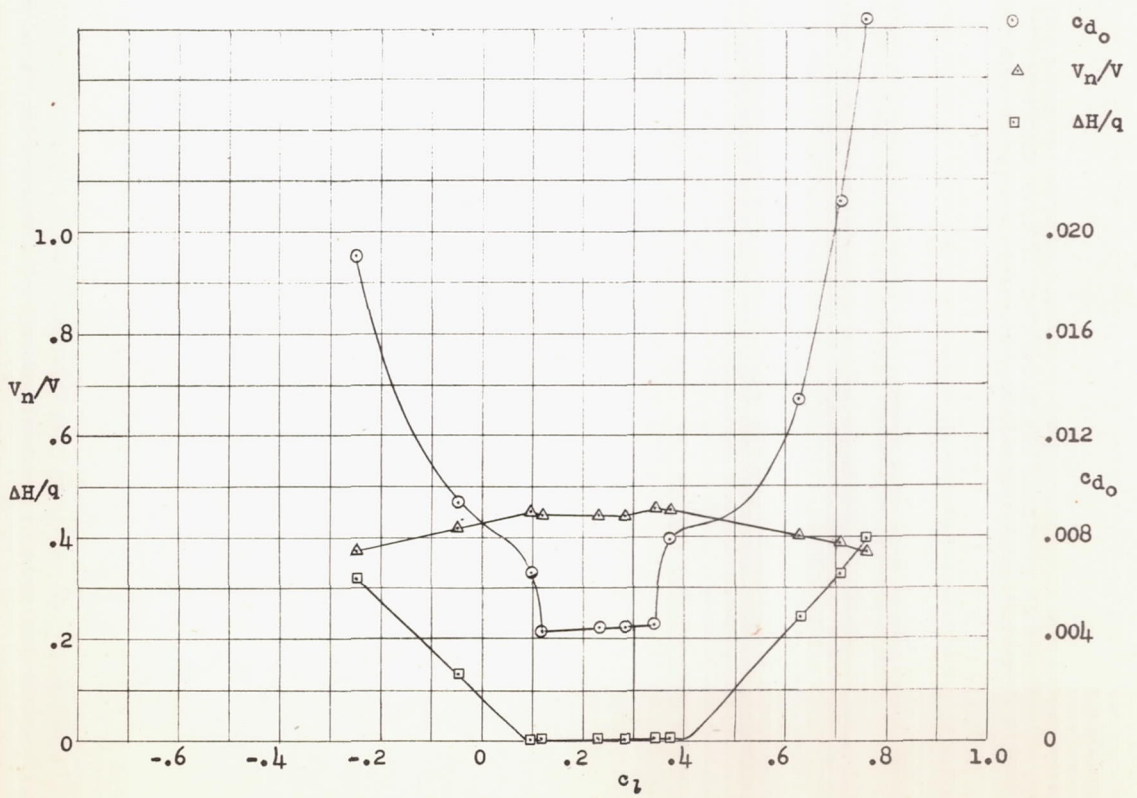

(b) A_t/A_n, 0.538.

L-694

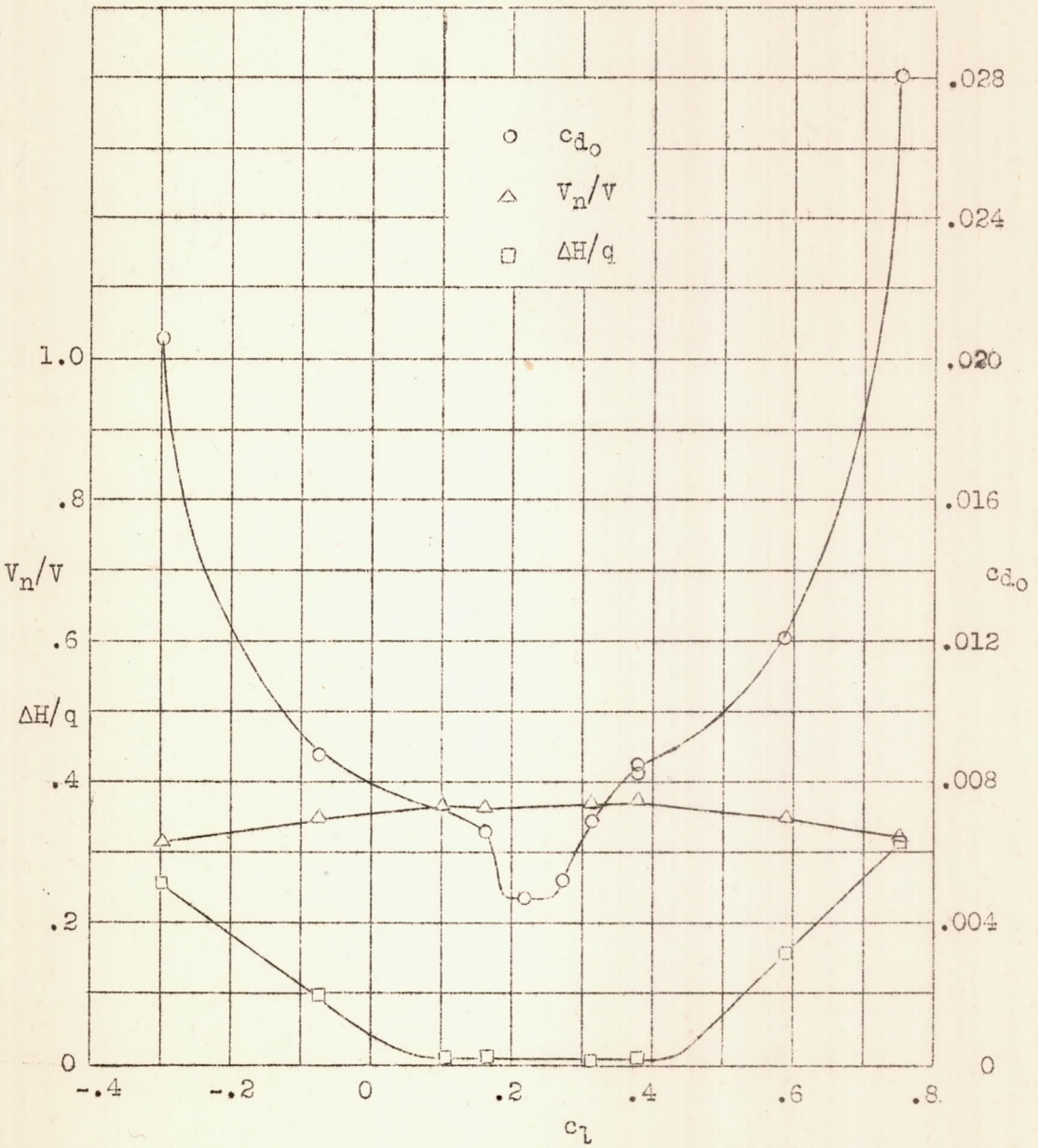

(c) A_t/A_n, 0.449.

Figure 16.- Concluded.

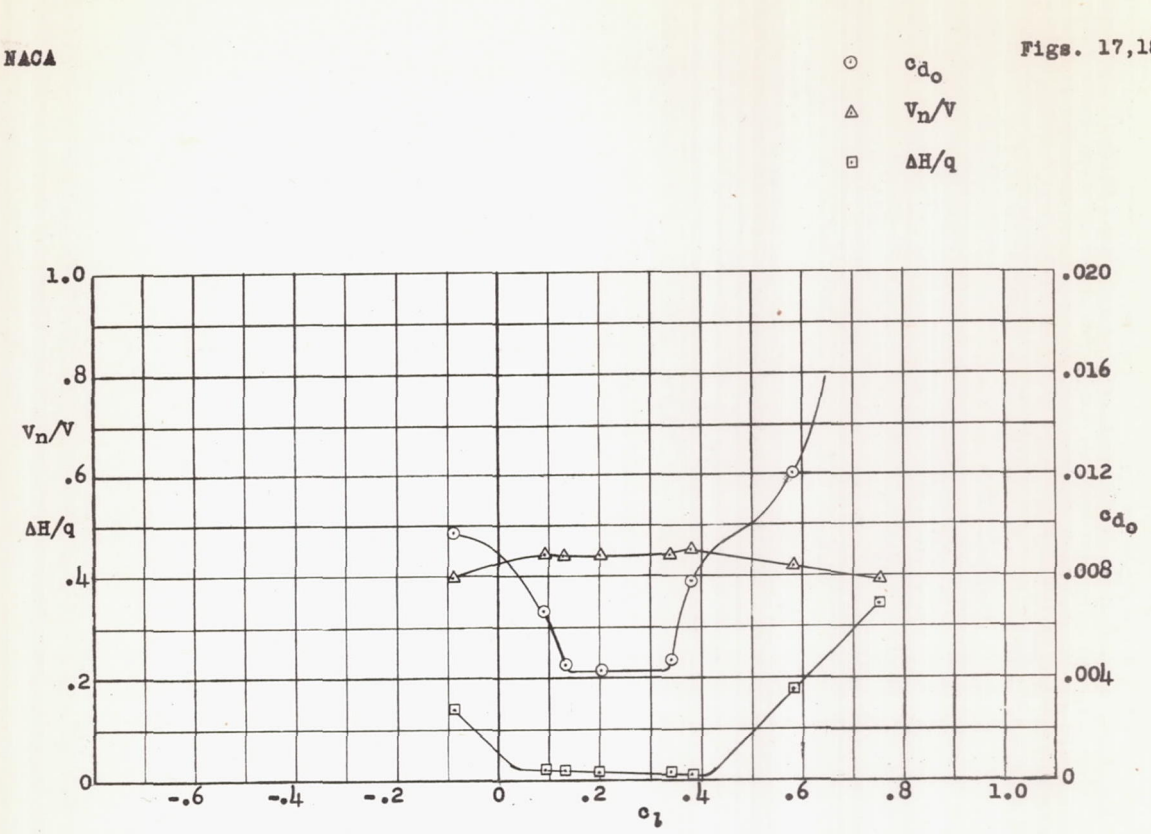

Figure 17.- Section characteristics for airfoil shape 10 at R = 6.43×10^6 and with a stagger of 0.53 inch. A_t/A_n, 0.538.

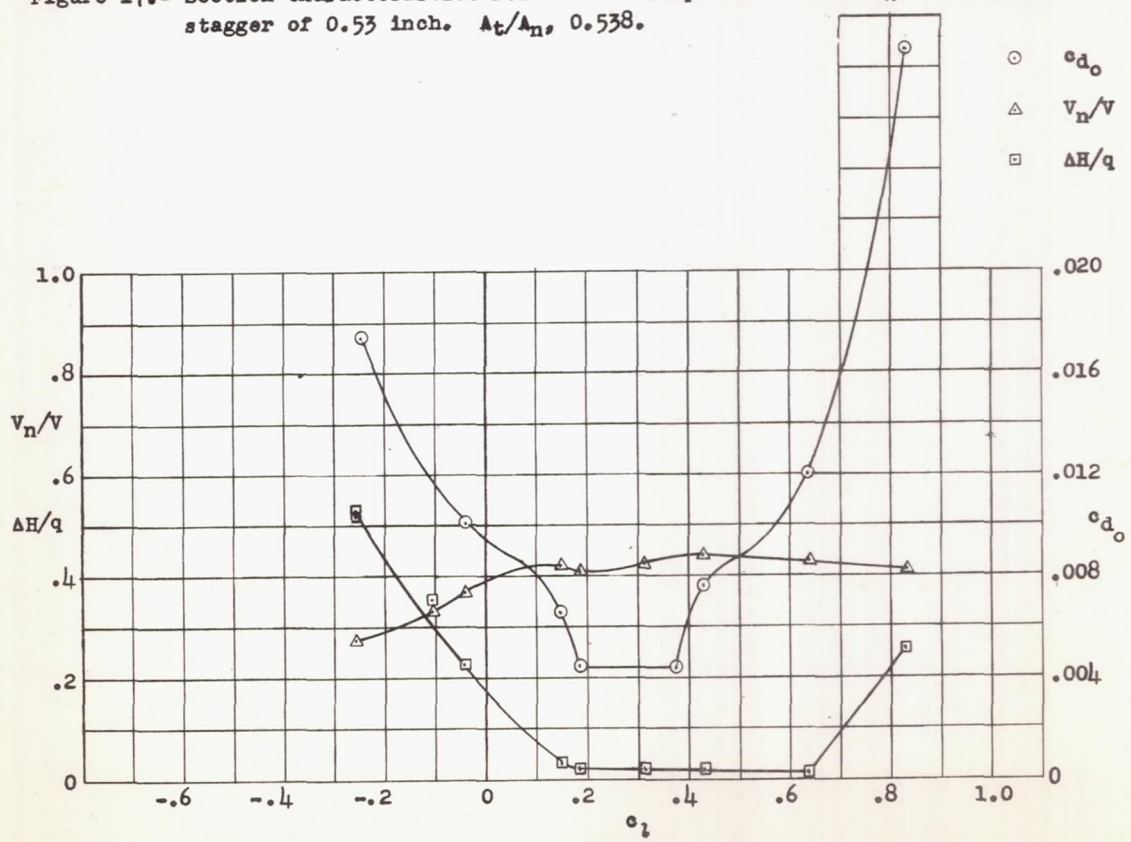

Figure 18.- Section characteristics for airfoil shape 10 at R = 6.43×10^6 and with a stagger of 1.10 inch. A_t/A_n, 0.538.

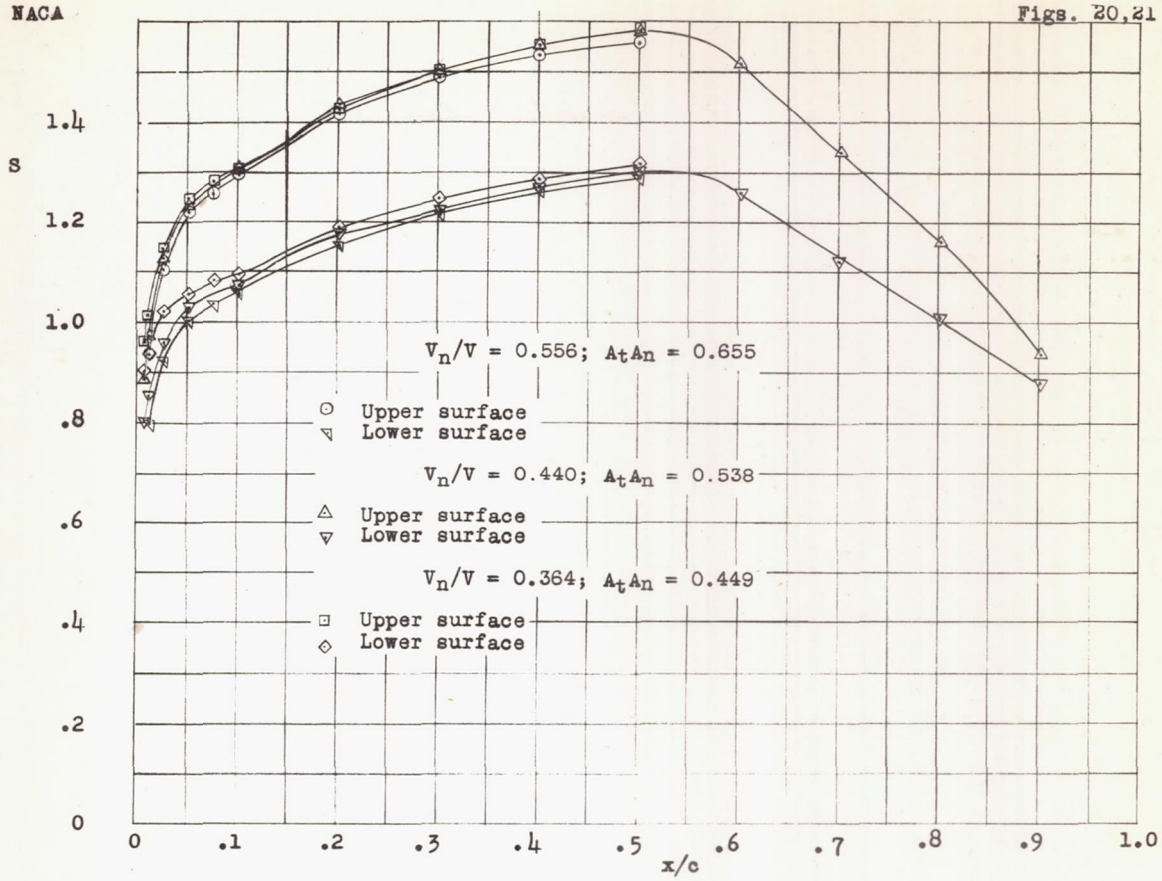

Figure 20.- Pressure distributions for airfoil shape 10. α, 0.55°; R, 6.43×10^6.

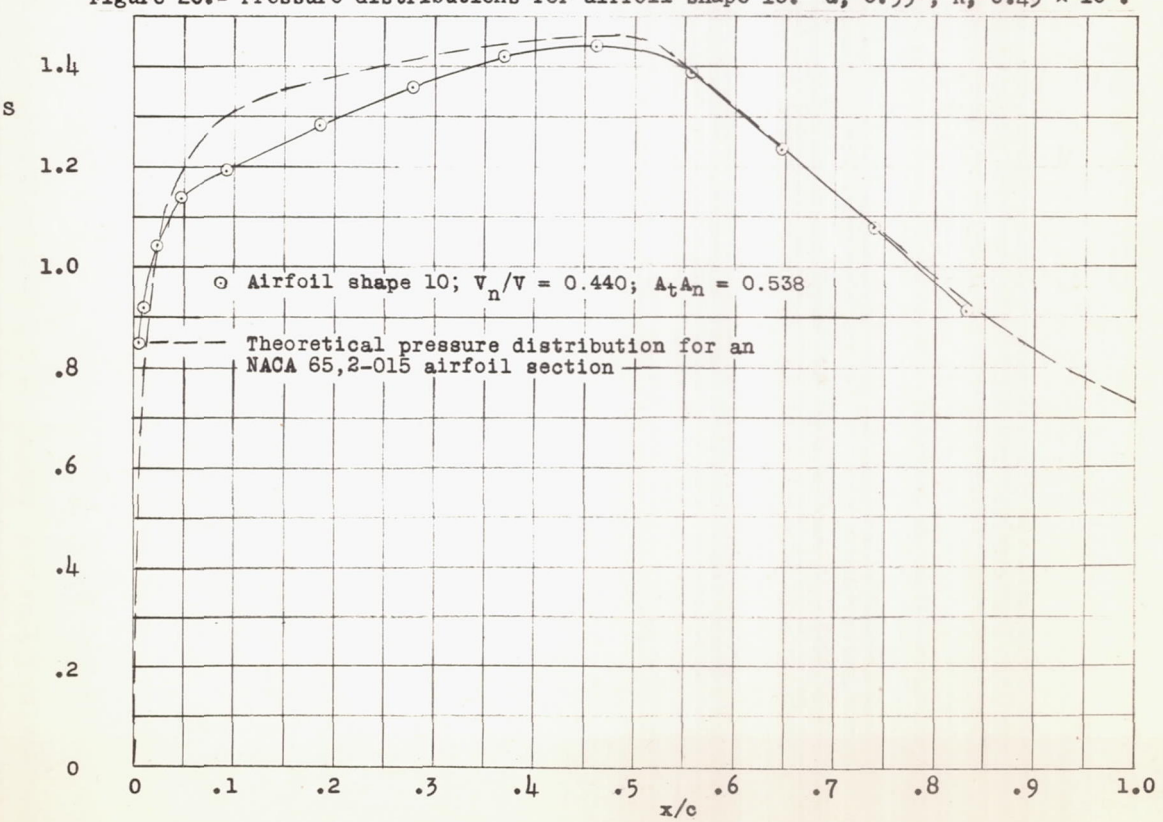

Figure 21.- Basic symmetrical pressure distribution for airfoil shape 10, derived from figure 20, compared with the theoretical pressure distribution for an NACA 65,2-015 airfoil section.

L-694

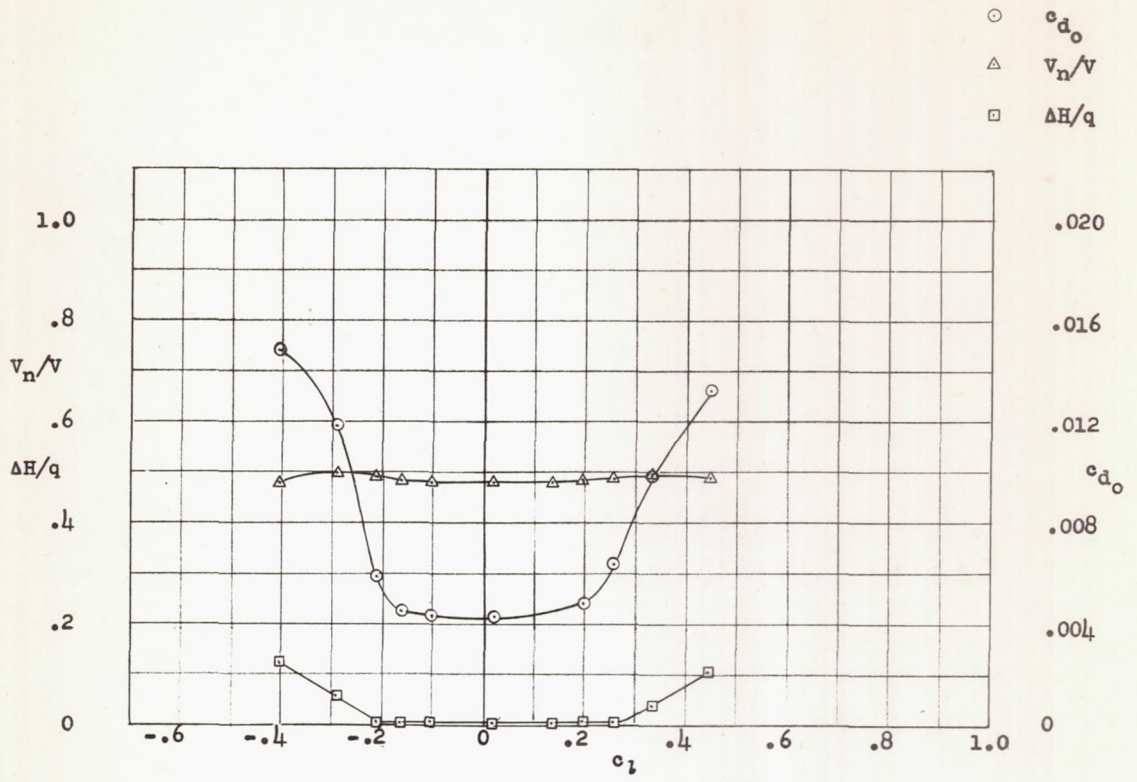

(a) A_t/A_n, 0.594.

Figure 22.- Section characteristics for airfoil shape 11. R, 6.43×10^6.

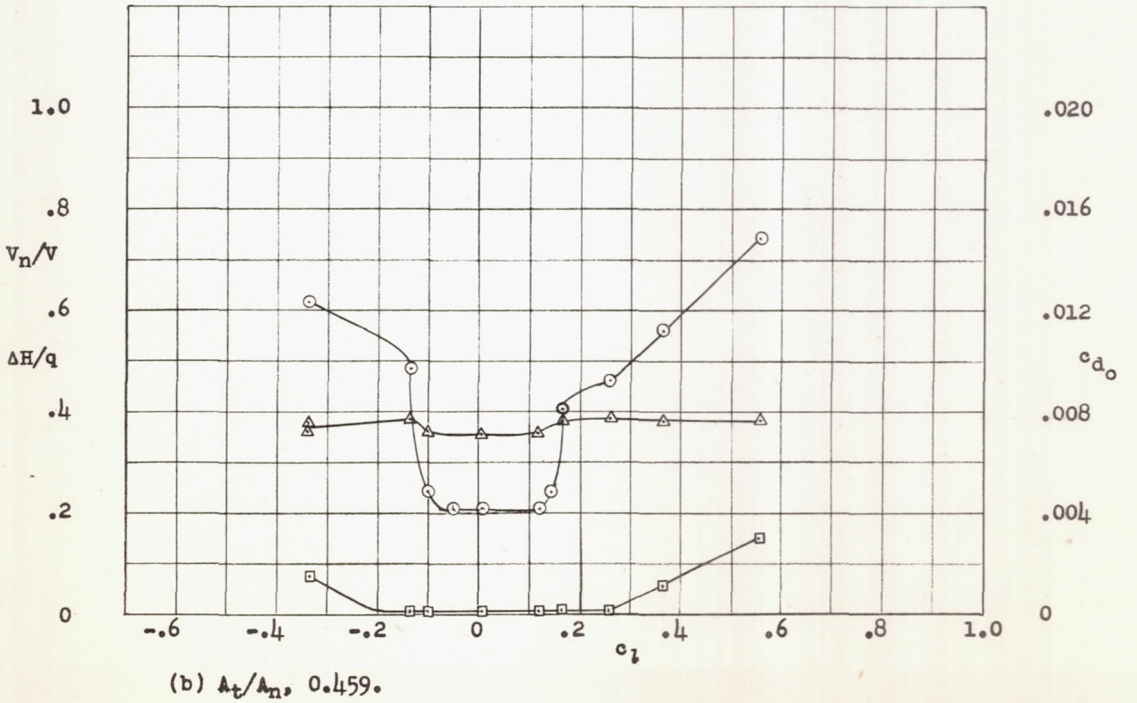

(b) A_t/A_n, 0.459.

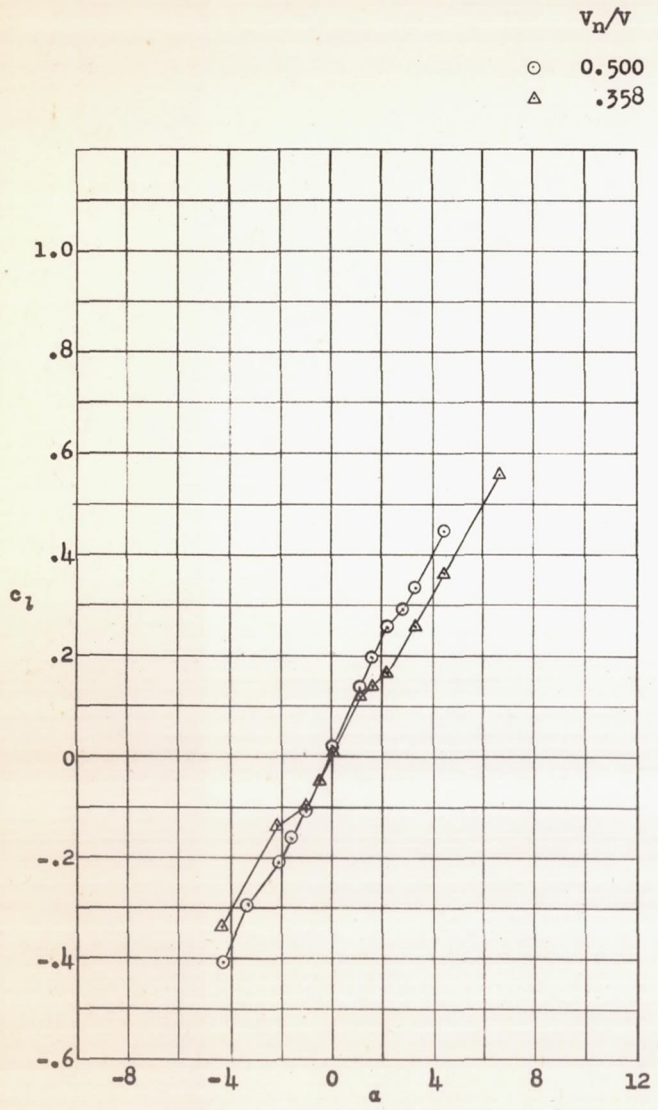

Figure 23.- Section lift coefficients for airfoil shape 11. R, 6.43×10^6.

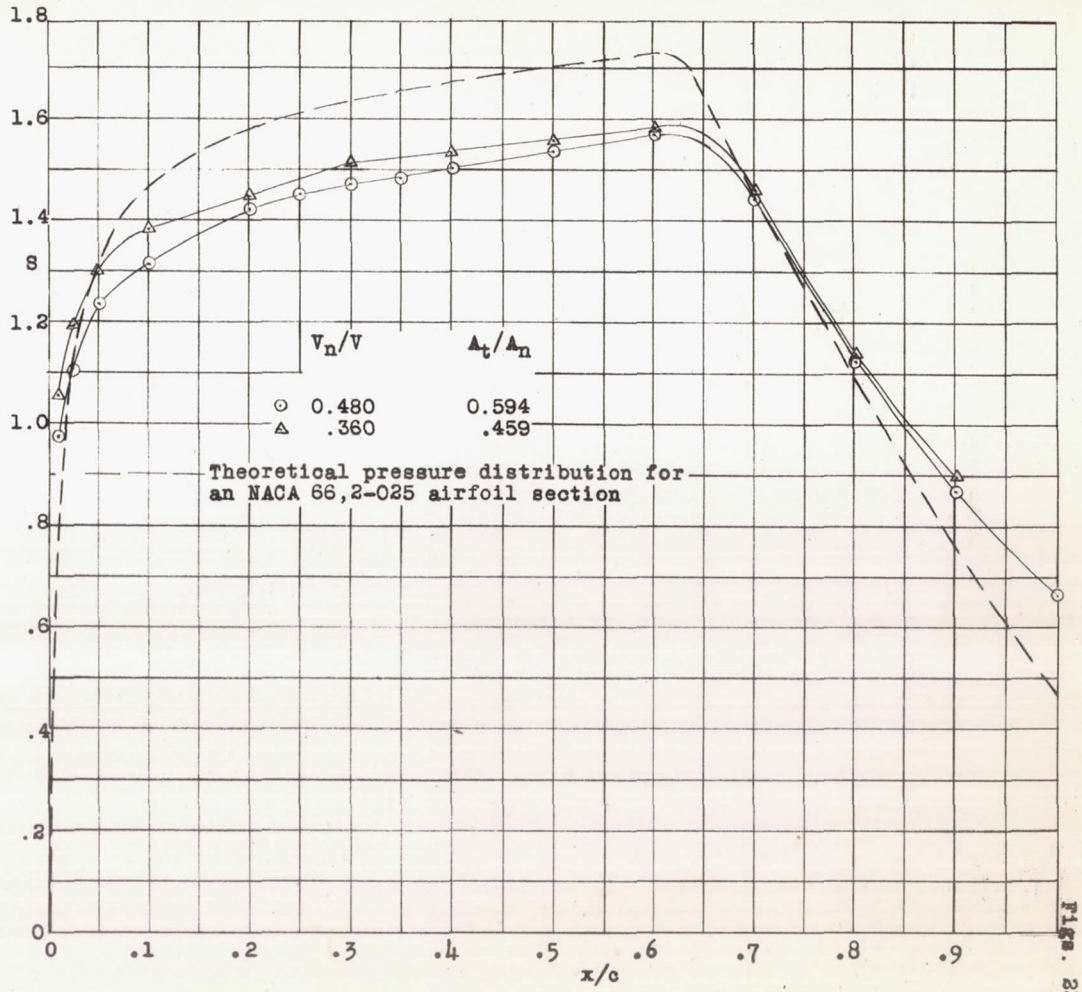

Figure 24.- Pressure distribution for airfoil shape 11. α, 0°; R, 6.43×10^6.

NACA

Figs. 23, 24

L-694

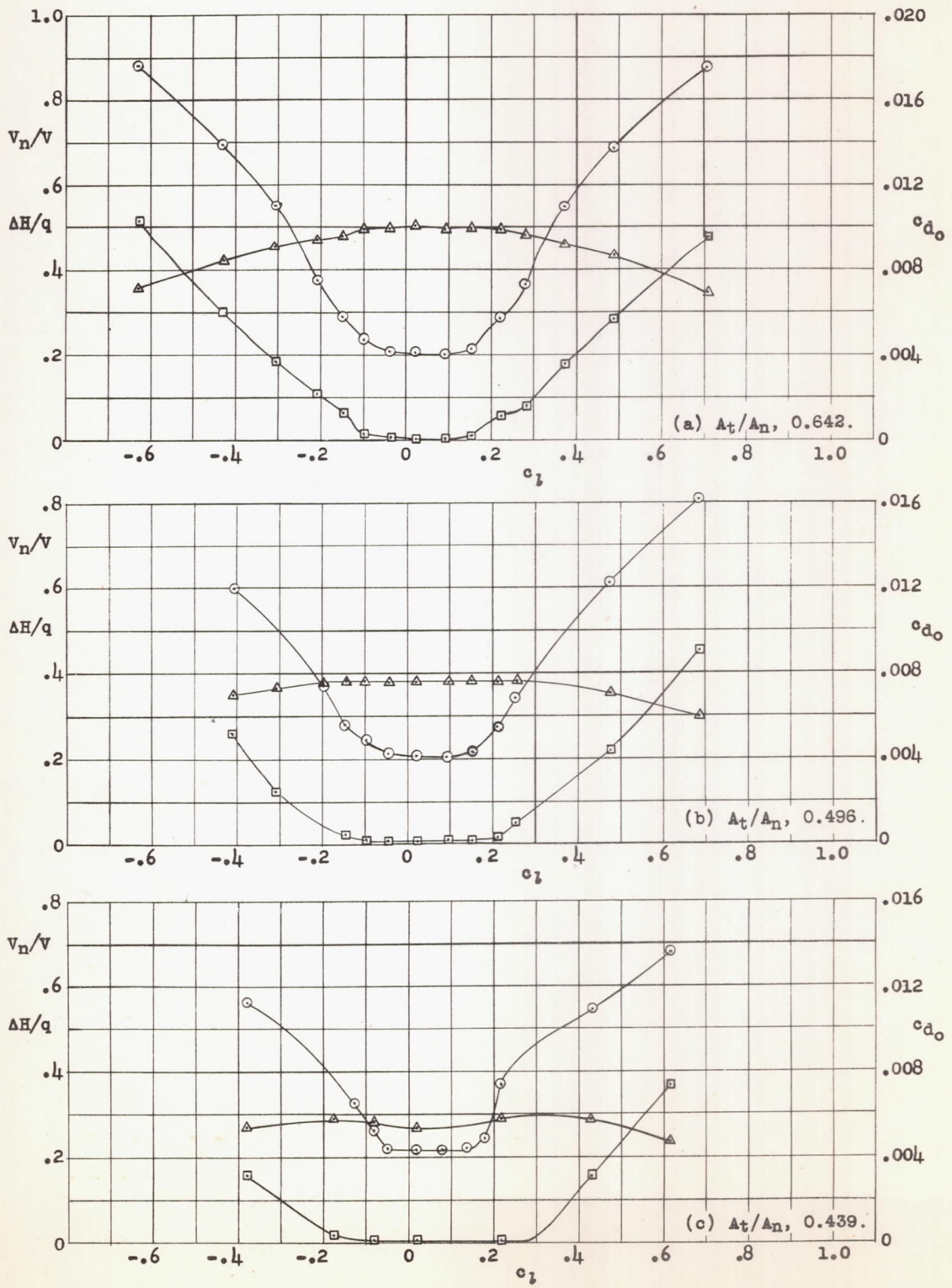

Figure 25.- Section characteristics for airfoil shape 12. R, 6.43×10^6.

L-684

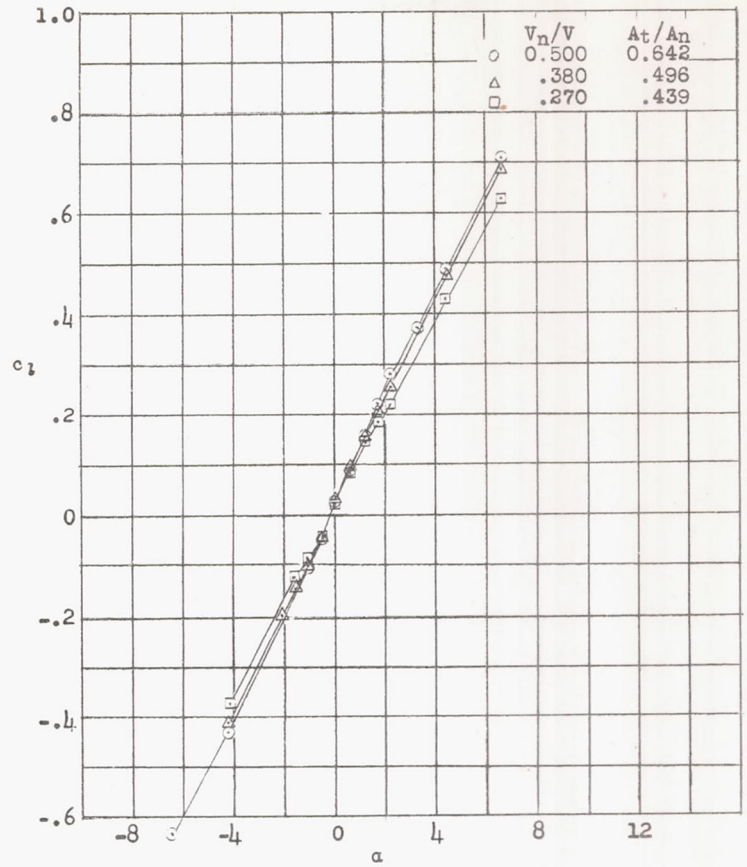

Figure 26.- Section lift coefficients for airfoil shape 12. R, 6.43×10^6.

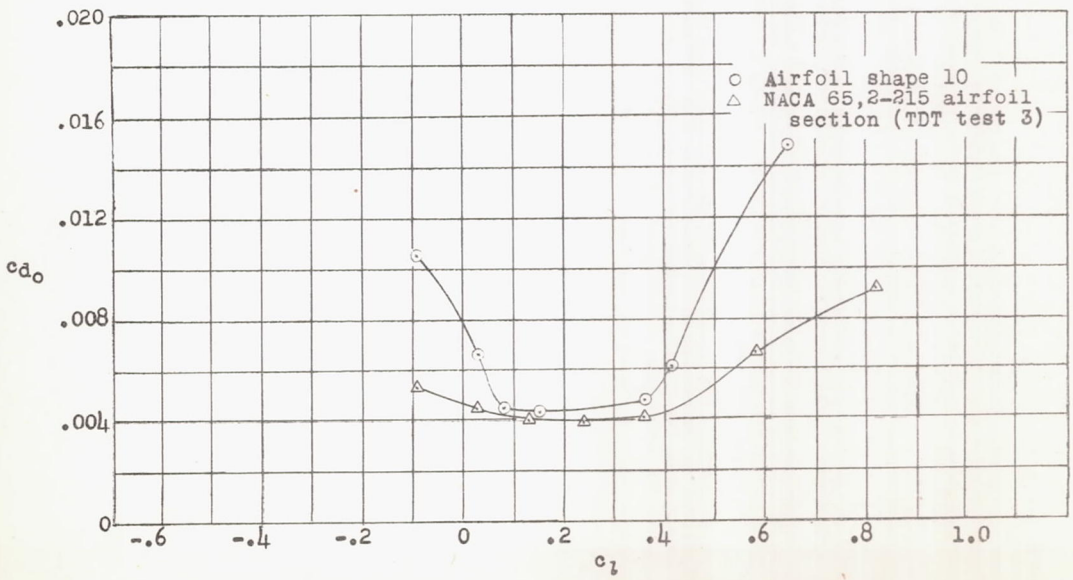

Figure 31.- Comparison of low-drag range for airfoil shape 10 from figure 16 and NACA 65,2-215 airfoil section, R, 6.7×10^6.

L-694

	V_n/V	A_t/A_n
⊙	0.500	0.642
△	.380	.496
⊡	.270	.439

——— Theoretical pressure distribution for an NACA 66,2-018.87 airfoil section.

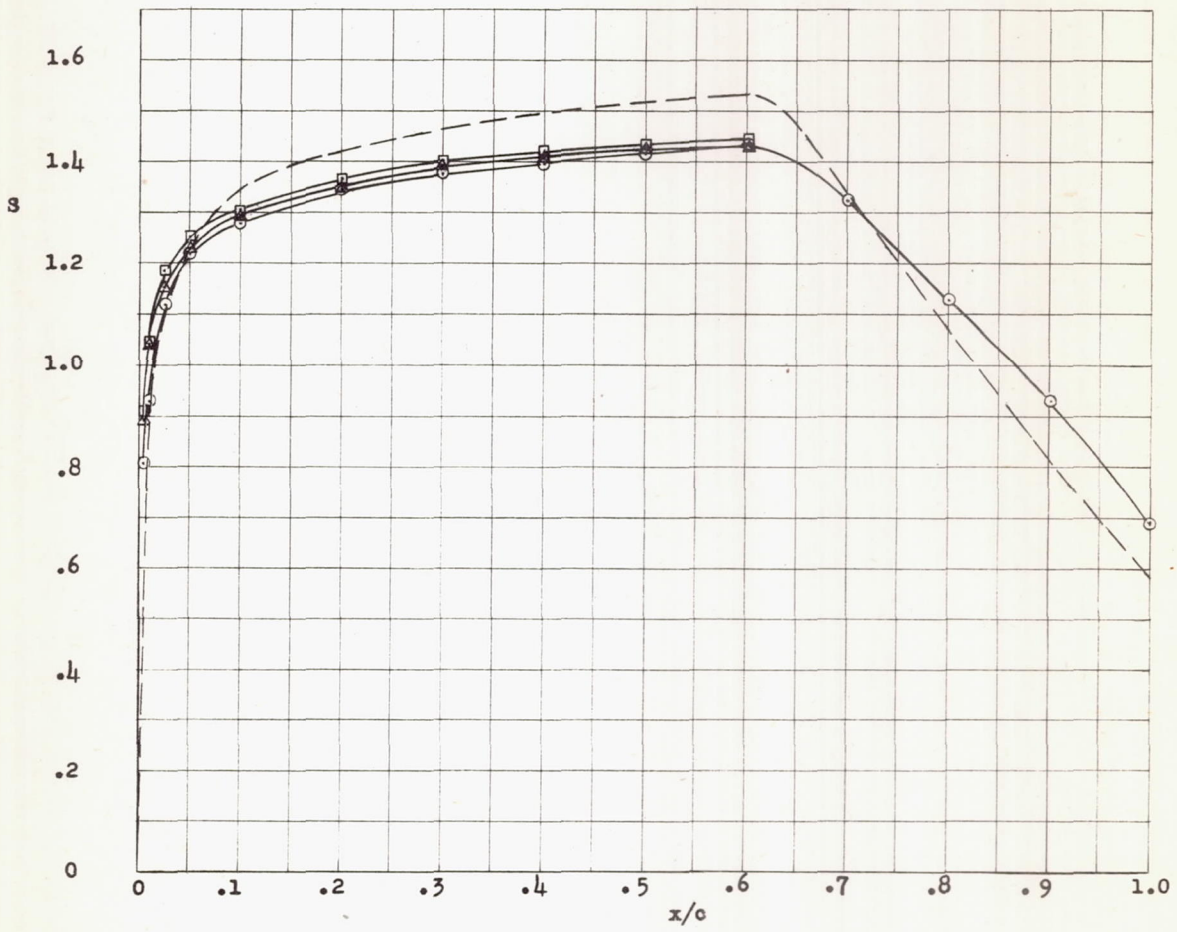

Figure 27.- Pressure distributions for airfoil shape 12. α, 0°; R, 6.43×10^6.

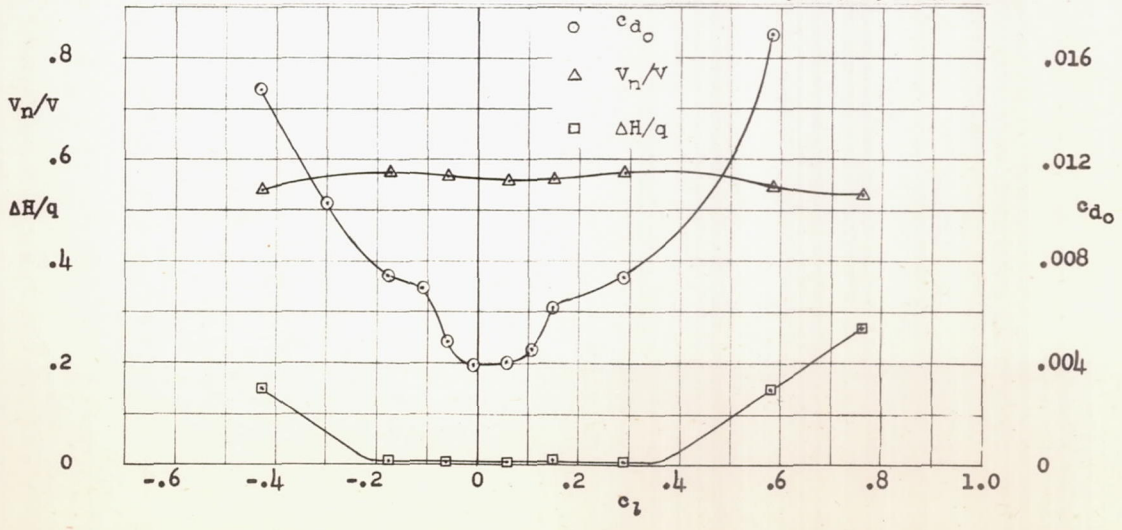

Figure 28.- Section characteristics for airfoil shape 13. A_t/A_n, 0.671; R, 6.43×10^6.

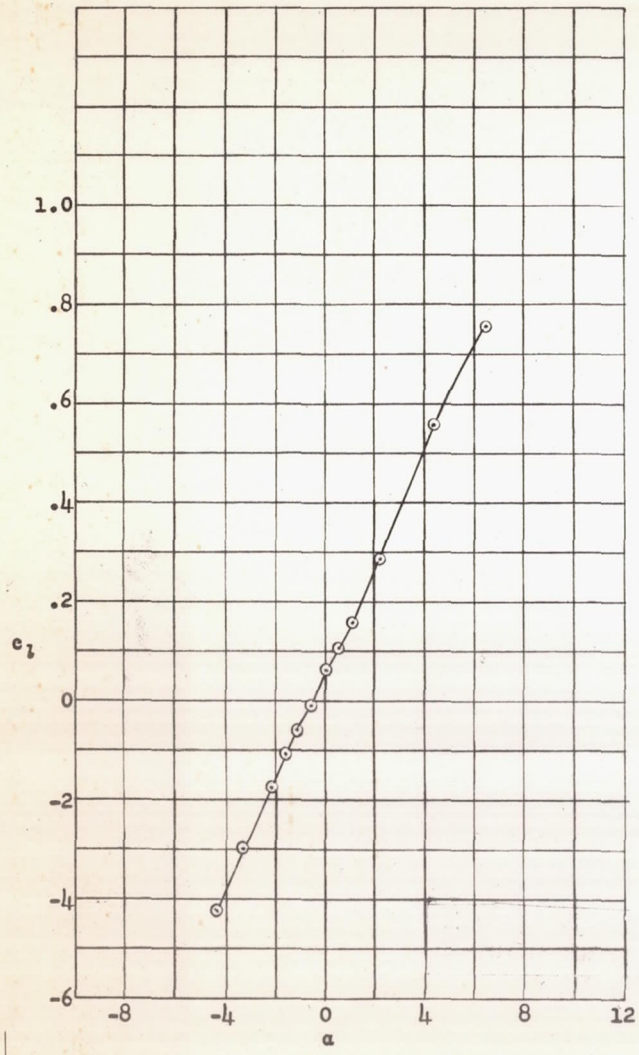

Figure 29.- Section lift coefficients for airfoil shape 13. V_n/V, 0.560; A_t/A_n, 0.671; R, 6.43 × 10^6.

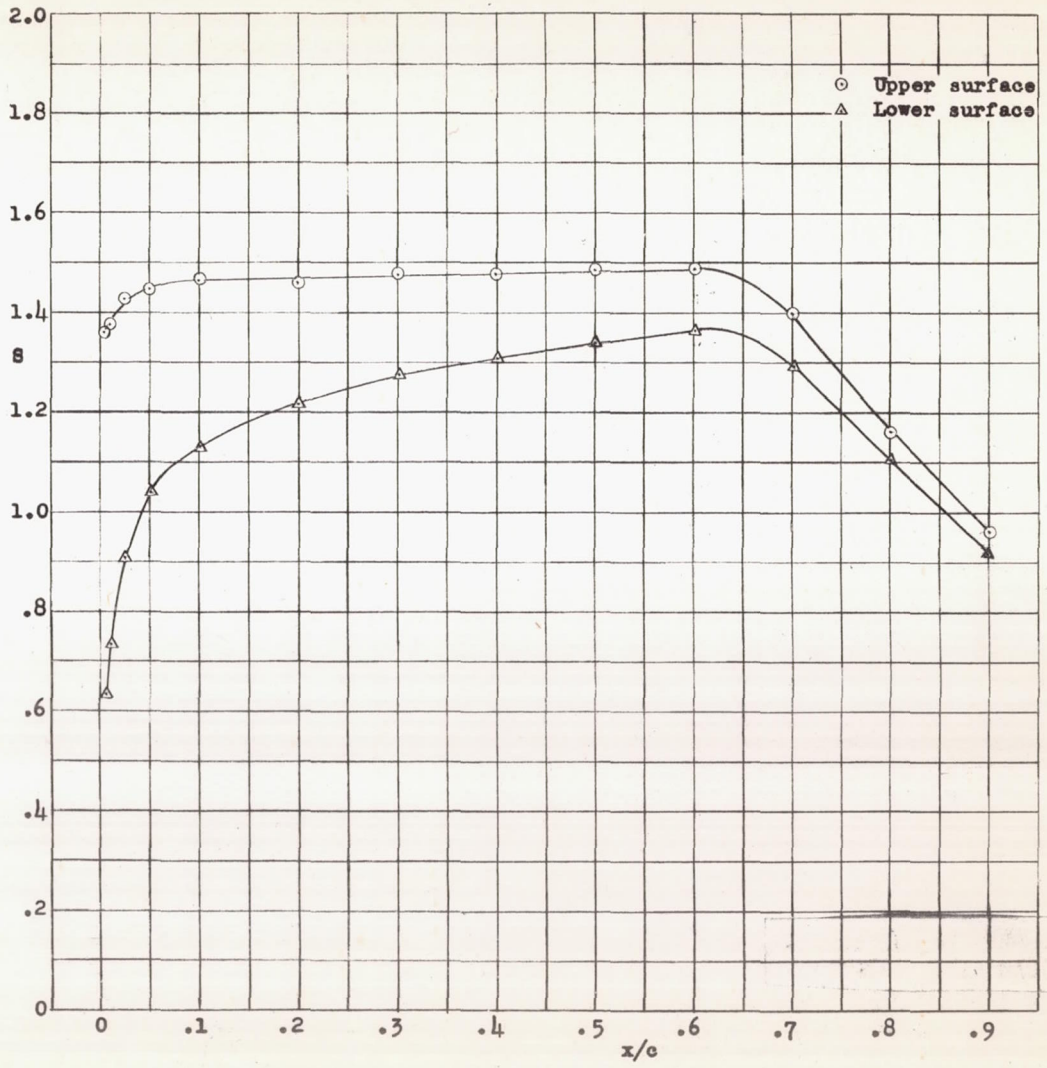

(a) α, 1.092°.

Figure 30.- Pressure distributions for airfoil shape 13. V_n/V, 0.560; A_t/A_n, 0.671; R, 6.43 × 10^6.
(a,b,c)

NACA

Figs. 29, 30a

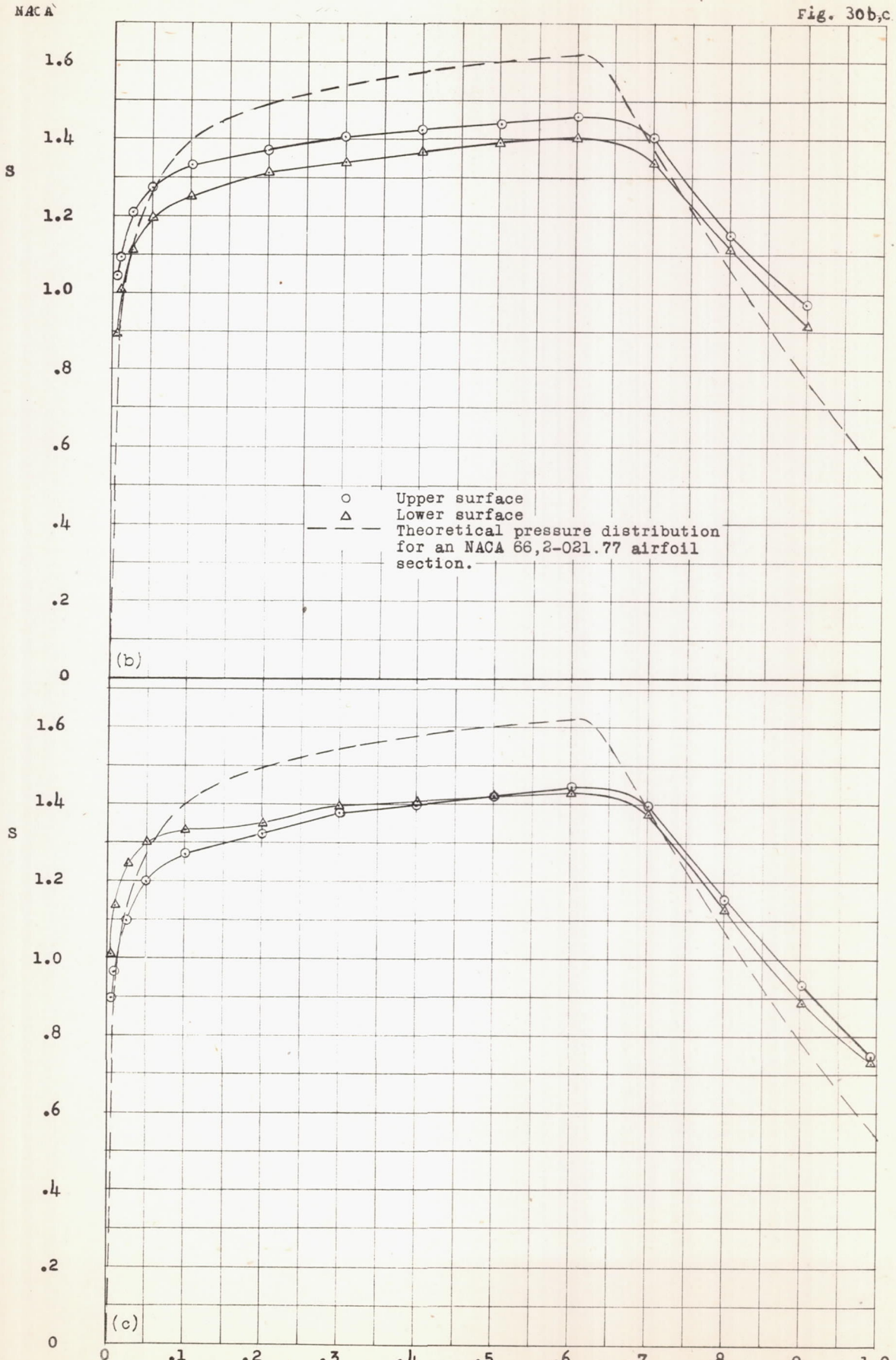

(b) o,0°; (c) o,0.55°.

Figure 30.- Concluded.